Vitamin D induces SIRT1 activation through K610 deacetylation in colon cancer

José Manuel García-Martínez[1], Ana Chocarro-Calvo[1], Javier Martínez-Useros[1,2], María Jesús Fernández-Aceñero[3], M. Carmen Fiuza[4], Jose Cáceres-Rentero[1], Antonio De la Vieja[5,6], Antonio Barbáchano[6,7,8], Alberto Muñoz[6,7,8], María Jesús Larriba[6,7,8] and Custodia García-Jiménez[1*]

[1] Area of Physiology, Faculty Health Sciences, University Rey Juan Carlos, 28922 Alcorcón, Madrid, Spain.

[2] Translational Oncology Division, OncoHealth Institute, Health Research Institute-University Hospital Fundación Jiménez Díaz-Universidad Autónoma de Madrid, 28040 Madrid, Spain.

[3] Department of Surgical Pathology, Hospital Clínico San Carlos, 28040 Madrid, Spain.

[4] Department of Surgery, University Hospital Fundación Alcorcón-Universidad Rey Juan Carlos, 28922 Alcorcón, Madrid, Spain.

[5] Unidad de Tumores Endocrinos (UFIEC), Instituto de Salud Carlos III, 28220 Majadahonda, Madrid, Spain.

[6] CIBER de Cáncer, Instituto de Salud Carlos III, Madrid, Spain.

[7] Instituto de Investigaciones Biomédicas "Alberto Sols", Consejo Superior de Investigaciones Científicas, Universidad Autónoma de Madrid, 28029 Madrid, Spain.

[8] Instituto de Investigación Sanitaria del Hospital Universitario La Paz, 28046 Madrid, Spain.

Running title: Vitamin D activates SIRT1 through deacetylation

Keywords: colorectal cancer; vitamin D; VDR; SIRT1; acetylation

* Correspondence: custodia.garcia@urjc.es; Tel.: +(34) 91 488 86 18

ABSTRACT

Posttranslational modifications of epigenetic modifiers provide a flexible and timely mechanism for rapid adaptations to the dynamic environment of cancer cells. SIRT1 is an NAD^+-dependent epigenetic modifier whose activity is classically associated with healthy aging and longevity, but its function in cancer is not well understood. Here, we reveal that 1α,25-dihydroxyvitamin D_3 (1,25$(OH)_2D_3$, calcitriol), the active metabolite of vitamin D (VD), promotes SIRT1 activation through auto-deacetylation in human colon carcinoma cells, and identify lysine 610 as an essential driver of SIRT1 activity. Remarkably, our data show that the post-translational control of SIRT1 activity mediates the antiproliferative action of 1,25$(OH)_2D_3$. This effect is reproduced by the SIRT1 activator SRT1720, suggesting that SIRT1 activators may offer new therapeutic possibilities for colon cancer patients who are VD deficient or unresponsive. Moreover, this might be extrapolated to inflammation and other VD deficiency-associated and highly prevalent diseases in which SIRT1 plays a prominent role.

INTRODUCTION

Over the last decades the study of genetic lesions in tumour cells provided key insights into the deregulated signalling pathways that promote cell proliferation and invasiveness and suppress senescence. In addition, increasing evidence from epidemiological studies suggests a significant impact of non-genetic modifiable factors on the oncogenic process by affecting cell epigenetics and thus, gene expression and phenotype. The key metabolic sensor SIRT1 acts an NAD^+-dependent deacetylase and a critical post-translational modifier and epigenetic regulator. As such, SIRT1 promotes efficient energy utilisation and cellular defences in response to environmental challenges, whereas its dysregulation accelerates age-related diseases such as diabetes and cancer (Bonkowski and Sinclair, 2016).

Colorectal cancer (CRC) is the second most diagnosed malignancy in women, the third in men, and a ~~major~~ leading cause of cancer-related deaths worldwide, with an incidence estimated to increase by 60% by 2030 (Bray et al., 2018; Cancer Genome Atlas Network, 2012). Many observational/epidemiological studies suggest that vitamin D (VD) deficiency is a risk factor for developing and dying of cancer, particularly for CRC (Feldman et al., 2014; Grant et al., 2022; Kim et al., 2022, 2021), albeit data from supplementation studies in the human population are controversial. Confirmation of a clinically relevant anti-CRC effect of VD in well-designed prospective randomized studies is still pending (Chandler et al., 2020; Henn et al., 2022; Manson et al., 2020; Muñoz and Grant, 2022; Song et al., 2021)

VD in humans has two origins: synthesis in the skin by the action of solar ultraviolet radiation on 7-dehydrocholesterol and the diet. The active VD metabolite is 1α,25-dihydroxyvitamin D_3 ($1,25(OH)_2D_3$, calcitriol), which results from two consecutive hydroxylations of VD, the first in the liver and the second in the kidney or in many epithelial and immune cell types (Bikle and Christakos, 2020; Feldman et al., 2014). VD actions are mediated by $1,25(OH)_2D_3$ binding to a member of the nuclear receptor superfamily of transcription factors,

74 the VD receptor (VDR). Upon ligand binding, VDR regulates the expression of hundreds of
75 target genes, many of which are involved in calcium and phosphate homeostasis, bone biology,
76 immune response, metabolism, detoxification, and cell survival, proliferation and differentiation
77 (Bikle and Christakos, 2020; Carlberg and Muñoz, 2022; Carlberg and Velleuer, 2022; Feldman
78 et al., 2014; Fernández-Barral et al., 2020).

79 Consistent with a protective role of VD against CRC, the colonic epithelium expresses
80 high levels of VDR. Many studies in CRC cells and associated fibroblasts and in experimental
81 animals have shown a large series of VDR-mediated VD anti-CRC effects (Carlberg and Muñoz,
82 2022; Carlberg and Velleuer, 2022; Feldman et al., 2014; Fernández-Barral et al., 2020; Ferrer-
83 Mayorga et al., 2019) In support, germline deletion of *Vdr* in mice with constitutively active
84 Wnt/β-catenin signalling, as a main driver of CRC, results in increased intestinal tumour load
85 (Larriba et al., 2011; Zheng et al., 2012).

86 Notably, certain evidence links SIRT1 and VD. First, decreased SIRT1 activity has been
87 linked to the pathogenesis of CRC (Ren et al., 2017; Strycharz et al., 2018). However, using
88 SIRT1 level as a marker of malignancy is controversial since both increased or decreased SIRT1
89 tumour expression have been described in different studies (Carafa et al., 2019; Chen et al., 2014;
90 Firestein et al., 2008), which points to a discrepancy between SIRT1 level and activity. Second,
91 SIRT1 deacetylates the VDR to enhance its activity in kidney and bone cells (Sabir et al., 2017)
92 and, consequently, decreased SIRT1 activity may drive VD insensitivity. Third, promoter-bound
93 VDR increases *SIRT1* gene expression in kidney and liver cells (Yuan et al., 2022) and thus, VD
94 deficiency may decrease SIRT1 levels leading to reduced activity. However, whether VD alters
95 SIRT1 activity *per se* and/or SIRT1 protein expression in CRC remains unclear.

96 Here we reveal that $1,25(OH)_2D_3$ induces specific SIRT1 activity at multiple levels in
97 human CRC cells. Notably, liganded VDR post-translationally increases SIRT1 activity through
98 auto-deacetylation. Mechanistically, SIRT1 K610 is identified as a critical player for

99 1,25(OH)$_2$D$_3$-enhanced VDR-SIRT1 interaction, SIRT1 auto-deacetylation and activation. This
100 occurs independently of increased SIRT1 RNA and protein expression and elevated cofactor
101 (NAD^+) levels. Discrepant SIRT1 level and activity may explain the controversial role of SIRT1
102 as tumor suppressor or tumor promoter in CRC. Our results provide a new mechanistic insight
103 into the association of VD deficiency with CRC and suggest potential therapeutic benefit for
104 SIRT1 activators in SIRT1-positive CRC.

105

106 **RESULTS**

107 ***1,25(OH)$_2$D$_3$ increases SIRT1 level via the VDR in CRC cells***

108 The question of whether VD governs SIRT1 activity in CRC was first approached in two
109 well characterized CRC cell lines, HCT 116 and HT-29. Immunofluorescence analyses (Fig.
110 1A) revealed that SIRT1 protein level doubled in response to 1,25(OH)$_2$D$_3$, a result confirmed
111 by Western blotting of nuclear extracts (Fig. 1B). The increased expression of SIRT1 protein by
112 1,25(OH)$_2$D$_3$ could be explained by a 2-fold upregulation of SIRT1 RNA revealed by RT-qPCR
113 (Fig.1C). The induction of *CYP24A1* (Fig. 1D), a major VDR target gene in many cell types
114 served as control for 1,25(OH)$_2$D$_3$ activity.

115 VDR expression is the main determinant of cell responsiveness to 1,25(OH)$_2$D$_3$ and is
116 downregulated in a proportion of patients with advanced CRC, implying that these patients
117 would probably not benefit from the anticancer effects of 1,25(OH)$_2$D$_3$ (Ferrer-Mayorga et al.,
118 2017; Larriba and Muñoz, 2005; Pálmer et al., 2004; Peña et al., 2005). To model CRCs patients
119 with low VDR tumour level or with VD deficiency, we used an HCT 116-derived cell line stably
120 depleted of VDR using shRNA (hereafter named ShVDR) (Larriba et al., 2011). Induction of
121 *SIRT1* gene expression by 1,25(OH)$_2$D$_3$ was confirmed by RT-qPCR analysis in ShControl but
122 not in ShVDR cells, although basal SIRT1 levels were similar (Fig. 1E). At the protein level,
123 confocal imaging showed reduced SIRT1 protein in ShVDR as compared to ShControl cells

124 (Fig. 1F), suggesting that VDR contributes to maintaining basal SIRT1 protein expression.
125 Western blot analyses on nuclear extracts confirmed that ShControl cells responded to
126 $1,25(OH)_2D_3$ with increased SIRT1 protein levels in contrast to the unresponsiveness of ShVDR
127 cells (Fig. 1G). Moreover, the upregulating effect of $1,25(OH)_2D_3$ was specific for SIRT1, since
128 the expression of the other nuclear sirtuin, SIRT7, was unaffected (Fig. 1H). Together, these data
129 indicated that $1,25(OH)_2D_3$ specifically increased SIRT1 mRNA and protein levels in CRC cell
130 lines via VDR. This is important because SIRT1 depletion and/or sirtuin activity decay might
131 represent an important neglected mediator of VD deficiency and a target for intervention in CRC.
132 Whether VD controls sirtuin activity independently of sirtuin level in CRC is a critical issue that
133 deserved further exploration.

134

135 ***$1,25(OH)_2D_3$ induces SIRT1 deacetylase activity in CRC cells***

136 Evaluation of global sirtuin activity in the nuclei of CRC cells revealed that treatment
137 with $1,25(OH)_2D_3$ increased NAD^+-dependent deacetylase activity 1.5-fold as compared to
138 control untreated cells (Fig. 2A). NAD^+ is a cofactor required for sirtuin activity. Metabolic
139 control of the level of NAD^+ represents an important node for sirtuin regulation and could explain
140 the induction of general sirtuin activity by $1,25(OH)_2D_3$. Indeed, nuclear NAD^+ level doubled in
141 response to $1,25(OH)_2D_3$ in human CRC cells (Fig. 2B). However, whether $1,25(OH)_2D_3$ could
142 specifically increase SIRT1 activity remained unknown.

143 Liganded VDR interacts with SIRT1 in kidney and bone cells (Sabir et al., 2017)
144 suggesting that $1,25(OH)_2D_3$ might alter SIRT1 expression or activity via post-transcriptional
145 mechanisms. Since protein-protein interactions regulate stability and activity of proteins, the
146 ability of $1,25(OH)_2D_3$ to promote VDR-SIRT1 interaction in CRC cells was evaluated by co-
147 immunoprecipitation assays. The results revealed that $1,25(OH)_2D_3$ potently (4-fold) enhanced
148 VDR/SIRT1 complex formation (Fig. 2C). To test if this interaction alters SIRT1 activity, the

149 acetylation status of two specific SIRT1 substrates (FOXO3a and H3K9) was evaluated as a read
150 out of SIRT1 deacetylase activity in response to $1,25(OH)_2D_3$. Acetyl-lysine
151 immunoprecipitation followed by Western blotting demonstrated efficient deacetylation of
152 FOXO3a in response to $1,25(OH)_2D_3$ (Fig. 2D). Likewise, the level of acetylated histone H3K9
153 (Ace H3K9) dramatically decreased in response to $1,25(OH)_2D_3$ (Fig. 2E), indicating specific
154 activation of SIRT1 by $1,25(OH)_2D_3$. The effect of $1,25(OH)_2D_3$ was mediated by VDR since
155 ShVDR cells did not show Ace H3K9 deacetylation in response to $1,25(OH)_2D_3$, whereas
156 ShControl cells maintained the response (Fig. 2F). Importantly, the specific SIRT1 activator
157 SRT1720 reduced Ace H3K9 levels in both ShControl and ShVDR cells, thus mimicking
158 $1,25(OH)_2D_3$ action independently of VDR (Fig. 2F).

159 The ability of $1,25(OH)_2D_3$ to increase protein deacetylation mediated by SIRT1 could
160 be driven either by elevated SIRT1 level or by increased SIRT1 activity. To distinguish between
161 these two possibilities, we performed an *in vitro* deacetylase assay using equivalent amounts of
162 immunoprecipitated SIRT1 from cells treated or not with $1,25(OH)_2D_3$. SIRT1-specific
163 deacetylase activity was enhanced 3-fold in cells treated with $1,25(OH)_2D_3$ despite similar levels
164 of immunoprecipitated SIRT1 (Fig. 2G).

165 Together, these results indicated that $1,25(OH)_2D_3$ induces nuclear SIRT1 activity. This
166 implies that VD deficiency and/or loss of tumour VDR expression (both observed in a proportion
167 of CRC patients) (Evans et al., 1998; Ferrer-Mayorga et al., 2019; Giardina et al., 2015; Larriba
168 et al., 2013, 2009; Pálmer et al., 2004; Peña et al., 2005) may negatively impact SIRT1
169 deacetylase activity and prompted us to examine samples of CRC patients.

170

171 ***CRC biopsies exhibit discrepancies between SIRT1 protein levels and deacetylase activity***

172 Changes in SIRT1 RNA and protein expression and enzymatic activity were analysed in
173 samples of CRC patients. First, we compared available data (TCGA-COAD database) from 160

174 pairs of human colon adenocarcinoma samples matched with their normal adjacent tissue. TNM
175 plot analysis revealed that both *VDR* and *SIRT1* gene expression decreased from normal to
176 tumour colonic tissue in a highly significant fashion ($P<0.001$) (Fig. 3A-B).

177 Immunohistochemical analysis of human colon tumor tissue microarrays (TMAs) from
178 the Biobank of Hospital Clínico San Carlos (HCSC, Madrid) revealed a significant ($P=0.017$)
179 positive association between the levels of VDR and SIRT1 proteins (Fig. 3C). An additional
180 TMA containing healthy colon samples was used to compare tumor and nontumor tissues. The
181 level of VDR protein was usually lower in tumour samples (Fig. 3D), while SIRT1 protein
182 expression showed high variability between tumors and high cellular intratumor heterogeneity
183 (Fig. 3D-E). Globally, TMA data suggested that SIRT1 protein levels in tumor samples (Fig.
184 3E), are subjected to high variability, which hampers statistical significance even though for
185 SIRT1 gene expression, differences were statistically significant as shown in Figure 3B.

186 Global acetylation also showed high cellular intratumor heterogeneity and variability
187 between samples without statistically significant differences between tumor and nontumor
188 samples (data not shown), showing that is not a valid, specific read out of SIRT1 activity. As an
189 alternative approach, the levels of SIRT1 protein and its substrate Ace H3K9 were compared
190 first in intestinal cell lines and then in human tumours. Surprisingly, SIRT1 protein level
191 increased in CRC cells as compared to normal HIEC6 cells (Fig. 3F). However, increased SIRT1
192 levels coincided with elevated Ace H3K9 (Fig. 3F), indicating SIRT1 inactivation in CRC cells.
193 The results in cell lines encouraged us to evaluate the potential discordance of SIRT1 and Ace
194 H3K9 levels in fresh-frozen samples from paired tumor and nontumor colonic tissue of patients
195 from Hospital Universitario Fundación Alcorcón (HUFA). All tissues were evaluated to have at
196 least 85% of tumor cells by immunohistochemistry (IHC). Western blotting allowed
197 simultaneous detection of SIRT1 and Ace H3K9. Notably, whereas the level of SIRT1 protein
198 variably increased or decreased from nontumor to tumor tissues in different patients, acetylation

199 of its specific substrate H3K9 consistently increased in tumor samples (Fig. 3G), reflecting
200 SIRT1 inactivation as found in carcinoma cell lines (Fig. 3F). *In vitro* deacetylation assays
201 performed on SIRT1 immunoprecipitated from SIRT1-positive patient samples confirmed a
202 common decrease of SIRT1 activity in colon tumor tissue (Fig. 3H). Western blotting illustrated
203 the variability of SIRT1 level among tumors and its correlation with VDR level (Fig. 3I), while
204 Ace H3K9 levels are generally high, but variable. Importantly, in vitro deacetylation assays on
205 SIRT1 immunoprecipitated from the same samples (Fig. 3J) confirmed Ace H3K9 as a *bona fide*
206 read out of SIRT1 inactivation. The discrepancy between the levels of SIRT1 protein expression
207 and activity in tumor samples may solve the controversy previously reported regarding the use
208 of SIRT1 as a tumor biomarker and poses the question of how $1,25(OH)_2D_3$ specifically enhances
209 SIRT1 deacetylase activity.

210

211 ***$1,25(OH)_2D_3$ induction of SIRT1 activity is mediated through auto deacetylation***

212 Since SIRT1 catalyses its auto deacetylation as a mechanism to increase its deacetylase
213 activity towards other substrates (Fang et al., 2017) and $1,25(OH)_2D_3$ facilitates VDR-SIRT1
214 interaction, we explored the possibility that liganded VDR increases SIRT1 activity by
215 facilitating SIRT1 auto deacetylation. To evaluate SIRT1 acetylation status upon exposure to
216 $1,25(OH)_2D_3$, nuclear extracts from CRC cells challenged or not with $1,25(OH)_2D_3$ were
217 immunoprecipitated using anti-acetyl-lysine antibodies and subjected to Western blotting.
218 $1,25(OH)_2D_3$ greatly reduced the nuclear pool of acetylated SIRT1 (Fig. 4A). Remarkably, the
219 specific SIRT1 activator SRT1720 also drove SIRT1 deacetylation in HCT 116 CRC cells (Fig.
220 4B). Consistently, ShVDR cells did not reduce acetylated SIRT1 in response to $1,25(OH)_2D_3$ but
221 retain their response to SRT1720 (Fig 4C). These results indicated that $1,25(OH)_2D_3$ activation
222 of SIRT1 is mediated through SIRT1 deacetylation.

223 Next, we sought to get further insight into the mechanism of regulation of SIRT1 activity
224 by 1,25$(OH)_2D_3$. As the acetyltransferase EP300 acetylates and inactivates SIRT2 (Han et al.,
225 2008) and is critical for CRC cell signalling (Chocarro-Calvo et al., 2013; Gutiérrez-Salmerón
226 et al., 2020), we used the ASEB engine (Wang et al., 2012) to search for SIRT1 residues
227 potentially acetylated by EP300. This approach identified K610, a lysine conserved from mouse
228 to human, as a potential EP300 target (Fig. 4D). The role of K610 in the regulation of SIRT1
229 activity was assessed by generating a non-acetylable K610R mutant, which should be resistant
230 to inactivation through acetylation. We compared the enzymatic activity of K610R SIRT1 with
231 that of wild type (WT) and inactive H363Y SIRT1 (Vaziri et al., 2001). Nuclear extracts from
232 cells transfected with MYC-tagged SIRT1 WT or mutants were immunoprecipitated using anti-
233 acetyl-lysine antibodies. Western blotting using an anti-MYC antibody revealed that exogenous
234 WT SIRT1 was acetylated (Fig. 4E), as it was endogenous SIRT1 (Fig 4A). Of note, catalytically
235 inactive H363Y SIRT1 was highly acetylated, in striking contrast with the lack of acetylation of
236 the K610R SIRT1 mutant (Fig. 4E), This highlights the importance of K610 for the regulation
237 of SIRT1 activity.

238 Since interaction with VDR was important for SIRT1 deacetylation activity, the ability
239 of each mutant to interact with VDR was compared in immunoprecipitation assays. The results
240 revealed that the K610R SIRT1 mutation facilitated the interaction with VDR, whereas the
241 inactive H363Y SIRT1 showed low interaction with VDR (Fig 4F). This suggested that
242 acetylation of SIRT1 might interfere with or destabilize its interaction with VDR, and that the
243 ability of 1,25$(OH)_2D_3$ to favour VDR-SIRT1 interaction may allow SIRT1 auto deacetylation,
244 and thus enhance its activity. The activity of mutant SIRT1 enzymes was first inferred from the
245 level of Ace H3K9, which was lower in cells expressing K610R SIRT1 (Fig 4G). *In vitro* NAD^+-
246 dependent deacetylase assays were next used to compare the activity of WT and mutant SIRT1.
247 Using equivalent amounts of immunoprecipitated MYC-tagged enzymes, we found a 10-fold

248 higher deacetylase activity for the K610R mutant than for WT SIRT1, whereas as expected the
249 H363Y inactive mutant exhibited very low activity as expected (Fig. 4H).

250

251 ***SIRT1 activation mimics the antiproliferative effects of 1,25(OH)$_2$D$_3$ in CRC cells***
252 ***unresponsive to VD***

253 Collectively, our data indicated that the acetylation status of SIRT1 K610 is critically controlled
254 and governs SIRT1 activity in the nuclei of CRC cells. By promoting VDR-SIRT1 interaction,
255 1,25(OH)$_2$D$_3$ facilitates SIRT1 auto deacetylation and enhances SIRT1 activity. These results
256 suggest that SIRT1 is an effector of 1,25(OH)$_2$D$_3$ and prompted us to ask whether the
257 pharmacological activation of SIRT1 would rescue CRC cells that are unresponsive to
258 1,25(OH)$_2$D$_3$.

259 The anticancer effects of 1,25(OH)$_2$D$_3$ are exerted at least partially through the inhibition
260 of tumor cell proliferation (Carlberg and Muñoz, 2022; Muñoz and Grant, 2022). 1,25(OH)$_2$D$_3$
261 strongly reduced the percentage of CRC cells in S-G$_2$M cell-cycle phases (Fig. 5A) and
262 consequently, it lengthened the cell cycle and reduced CRC cell proliferation. We aimed to
263 analyse the effect of the modulation of SIRT1 activity on the proliferation of CRC cells and on
264 the antiproliferative action of 1,25(OH)2D3. Inhibition of general sirtuin activity with
265 Nicotinamide (NAA) abolished the antiproliferative effects of 1,25(OH)$_2$D$_3$ on CRC cells (Fig.
266 5B). Moreover, activation of SIRT1 by the small molecule SRT1720 mimicked the response to
267 1,25(OH)$_2$D$_3$ and efficiently reduced the percentage of cells in S-G$_2$M cell cycle phases (Fig.
268 5C). These data indicate that induction of SIRT1 activity mediates 1,25(OH)$_2$D$_3$-driven cell cycle
269 lengthening in CRC cells.

270 As expected, in contrast with ShControl cells, ShVDR CRC cells did not extend the cell
271 cycle in response to 1,25(OH)$_2$D$_3$ (Fig. 5D). Accordingly, an early and strong reduction in the
272 proliferation rate in response to 1,25(OH)$_2$D$_3$ was noted in ShControl cells but it was almost

273 absent in ShVDR cells (Fig. 5E). Specific SIRT1 activation with SRT1720 reduced the
274 proliferation of ShControl cells at a comparable magnitude to $1,25(OH)_2D_3$ and, importantly,
275 also reduced proliferation of $1,25(OH)_2D_3$-unresponsive ShVDR cells (Fig.5E).

276 Collectively, these results show that SIRT1 acts downstream of $1,25(OH)_2D_3$-activated
277 VDR in the inhibition of CRC cell proliferation. They also suggest that activation of SIRT1 in
278 CRC patients with vitamin D deficiency or with VD unresponsive tumors (conditions frequently
279 observed in advanced CRC), could be a therapeutic strategy to effectively antagonize cell
280 proliferation.

281

282 **DISCUSSION**

283 Here we reveal that $1,25(OH)_2D_3$ activates the epigenetic regulator SIRT1 by acting at
284 multiple levels. Ligand-activated VDR post-translationally upregulates SIRT1 activity by
285 facilitating its auto deacetylation. Mechanistically, SIRT1 K610 is identified as essential to
286 control VDR-SIRT1 interaction and SIRT1 acetylation status and activity. Notably, both
287 SRT1720 and $1,25(OH)_2D_3$ activate SIRT1 through auto deacetylation. Modulation of SIRT1
288 activity by $1,25(OH)_2D_3$ through deacetylation occurs in addition to increased mRNA and
289 protein levels as well as to an elevation of cofactor (NAD^+) availability. Thus, $1,25(OH)_2D_3$
290 activates SIRT1 acting at multiple levels, from gene expression to activity, and these findings
291 broaden our understanding of how VD deficiency is associated with CRC.

292 We also show that SIRT1 deacetylase activity mediates the anti-proliferative action of
293 $1,25(OH)_2D_3$ in CRC, which is in line with the recent proposal that SIRT1 activity opposes
294 several cancer cell hallmarks (Yousafzai et al., 2021). In cases of VD deficiency and/or
295 unresponsiveness such as advanced colorectal tumor lacking VDR expression due to
296 transcriptional repression by SNAIL1/2 (Pálmer et al., 2004; Larriba et al., 2009), the activation
297 of SIRT1 by compounds other than $1,25(OH)_2D_3$ may be especially relevant. Clinical trials that

298 explore SIRT1 activators in CRC are rare (https://clinicaltrials.gov). Some trials are designed to
299 study doses and pharmacokinetics of resveratrol, a known sirtuin activator that has many other
300 targets (Patel et al., 2011). Currently there are not known clinical trials using SRT1720 or
301 alternative SIRT1 specific activators.

302 Consideration of SIRT1 protein level as a prognostic marker for cancer has received
303 much attention, but conflicting results reporting both, tumor SIRT1 increases and decreases
304 raised controversy (Ren et al., 2017; Wu et al., 2017). Accordingly, some studies propose SIRT1
305 either as tumour suppressor or as tumor promoter in CRC (Carafa et al., 2019; Ren et al., 2017).
306 Importantly, SIRT1 protein level might not always reflect SIRT1 activity, and some tumors could
307 possibly increase SIRT1 protein expression to counteract inactivation. Our results, which
308 indicate the existence of discrepancies between SIRT1 levels and activity in human colorectal
309 tumors, may help to resolve the controversy. Interestingly, alternative posttranslational SIRT1
310 modifications may have a similar outcome. For example, proteolytic cleavage of SIRT1 induced
311 by TNFα in osteoarthritis renders accumulation of a catalytically inactive 75 kDa resistant
312 fragment (Oppenheimer et al., 2012) that could be detected by immunohistochemistry. Since
313 inflammation (in general) and especially TNFα is an important mediator of CRC, understanding
314 if this fragment is generated in CRC patients and whether its presence would also lead to
315 decreased SIRT1 activity in samples strongly positive for SIRT1 remains as an interesting
316 unexplored issue.

317 The ability of $1,25(OH)_2D_3$ to activate SIRT1 may have further major implications for
318 physiological and pathological processes other than CRC since SIRT1 target proteins control
319 several processes such as mitochondria physiology, apoptosis, and inflammation (Strycharz et
320 al., 2018). Thus, $1,25(OH)_2D_3$ may not only regulate gene expression via direct transcriptional
321 regulation of VDR-bound targets, but it can secondarily impact a wide range of events and
322 processes via the control of SIRT1 activity. This may explain how $1,25(OH)_2D_3$ regulates the

323 activity of FOXO3a, an important modulator of cell proliferation and the immune response that
324 is targeted by SIRT1 (An et al., 2010). SIRT1 also modulates the activity of the tumour
325 suppressor p53, whose mutation is a relatively early event in a high proportion of CRCs (Polidoro
326 et al., 2013; Strycharz et al., 2018). In this way, SIRT1 activation greatly broaden the known
327 vitamin D regulatory action, albeit whether $1,25(OH)_2D_3$ directs SIRT1 activity towards specific
328 substrates remains to be elucidated. The accumulating evidence for SIRT1 involvement in
329 chronic inflammation (Mendes et al., 2017) suggests a potential benefit of SIRT1 activation by
330 $1,25(OH)_2D_3$ in chronic inflammation-linked CRC and other diseases. Moreover, the mechanism
331 revealed here for SIRT1 activation by $1,25(OH)_2D_3$ may be relevant for diseases associated with
332 VD deficiency beyond CRC, including autoimmune disorders and diabetes.

333 In conclusion, the multilevel activation of SIRT1 deacetylase by $1,25(OH)_2D_3$ broadens
334 the range of known $1,25(OH)_2D_3$ targets and positions SIRT1 as an important mediator of the
335 protective action of VD against CRC and potentially other neoplasias and non-tumoral diseases.
336 These data support SIRT1 activators as useful agents in situations of dysfunction of the VD
337 system.

338

339 **MATERIALS AND METHODS**

340 All materials and resources can be found in Table 1.

341

342 **Experimental model and subject details**

343 **Human samples**

344 Patient samples were derived from surgical removal at Fundación Jimenez Diaz University
345 Hospital, General and Digestive Tract Surgery Department: 95 patient samples diagnosed with
346 stage II CRC. The Institutional Review Board (IRB) of the Fundación Jimenez Diaz Hospital,
347 reviewed and approved the study, granting approval on December 9, 2014, act number 17/14.

348 Samples from seven healthy individuals were obtained from Hospital Clínico San Carlos
349 (HCSC). IRB-HCSC act number 21/498-E granting approval on June 25th, 2021. Paired fresh-
350 frozen samples from tumor and nontumor adjacent tissue were collected from 18 patients at
351 Hospital Universitario Fundación Alcorcón (HUFA). IRB-HUFA, act number 17/68 granting
352 approval on June 8th, 2017. Colon cancer tissues were collected using protocols approved by the
353 corresponding Ethics Committees and following the legislation. All patients gave written
354 informed consent for the use of their biological samples for research purposes. Fundamental
355 ethical principles and rights promoted by Spain (LOPD 15/1999) and the European Union EU
356 (2000/C364/01) were followed. All patients' data were processed according to the Declaration
357 of Helsinki (last revision 2013) and Spanish National Biomedical Research Law (14/2007, July
358 3).

359 **Colorectal cell panels**

360 Human colorectal adenocarcinoma HT-29 and HCT 116 and HCT 116 derived ShControl and
361 ShVDR cells were cultured under standard conditions, in 5%CO2 at 37ºC with DMEM
362 containing 25 mM glucose (unless specifically indicated) and 40 mM LiCl to mimic Wnt
363 signalling and supplemented with 10% foetal bovine serum (FBS) and 1% penicillin-
364 streptomycin. Cells were treated as indicated for 24h. HCT 116 ShControl and ShVDR cell lines
365 were derived previously (Larriba et al., 2011)

366 **Transient transfections**

367 cells were seeded in plates at 50% confluence for plasmid transfection, using JetPei PolyPlus
368 reagent (Genycell Biotech), following the manufacturer's instructions. After 24 h cells were
369 treated as indicated for 24 h.

370 For Sirt1 siRNA, cells plated in six well plates at 50% confluence were transfected with
371 JetPRIME PolyPlus reagent (Genycell Biotech) following the manufacturer's instructions. After

372 2 days cells were treated 24 h with LiCl and then another 24 h with 1,25$(OH)_2D_3$ before
373 harvesting to analyse by western blot.

374 **Site directed mutagenesis**

375 Directed mutagenesis was performed using the QuickChange Site-Directed Mutagenesis Kit
376 (Stratagene). Oligonucleotides containing the mutation (Table 1) were designed following the
377 manufacturer's recommendations. 2.5 U of PfuTurbo DNA polymerase was added to each
378 sample and they were amplified by performing the following cycles: 1 denaturation cycle at 95 °
379 C for 1 minute, 18 amplification cycles of 30 seconds at 95 ° C, 50 seconds at 60 ° C, 1 minute
380 / kilobase of plasmid at 68 °C and the last extension cycle 7 minutes at 68ªC. Once amplified, 10
381 U of Dnp I enzyme were added and incubated at 37 ° C for one hour to digest the supercoiled
382 double-stranded DNA and eliminate the parental molecules that are not mutated.

383 The correct introduction of the mutation was evaluated by plasmid sequencing using the BigDye
384 Cycle Sequencing Kit (Applied Biosystems).

385 **Preparation of cell extracts:**

386 Whole cell extracts.

387 Cells were washed with iced PBS before extract preparation and scraped in RIPA buffer (10 mM
388 Tris HCl [pH 7.4], 5 mM EDTA, 5 mM EGTA, 1% Tryton X100, 10 mM $Na_4P_2O_7$ [pH 7.4], 10
389 mM NaF, 130 mM NaCl, 0.1% SDS, 0,5% Na-deoxycholate). After 5 min on ice, cells were
390 pelleted (12000 rpm for 5 min, 4ºC) and the supernatant was directly used as whole cell extract
391 or frozen at -80 ºC.

392 Fractionated cell extracts.

393 After washing as before, cells were scraped in hypotonic buffer (20 mM Hepes, [pH 8.0], 10 mM
394 KCl, 0,15 mM EDTA, 0,15 mM EGTA, 0,05% NP40 and protease inhibitors) and incubated on
395 ice for 10 min before adding 1:2 vol of sucrose buffer (50 mM Hepes [pH=8.0], 0.25 mM EDTA,
396 10 mM KCl, 70% sucrose). Lysates were fractionated (5000 rpm for 5 min at 4ºC) to obtain the
397 cytoplasmic fraction in the supernatant. Nuclear pellets were washed twice with washing buffer

398 (20 mM Hepes [pH 8.0], 50 mM NaCl, $MgCl_2$ 1.5 mM, 0,25 mM EDTA, 0,15 mM EGTA, 25%
399 glycerol and protease inhibitors), pelleted at 5000 rpm, 5 min at 4ºC and resuspended in nuclear
400 extraction buffer (20 mM Hepes[pH 8.0], 450 mM NaCl, $MgCl_2$ 1.5 mM, 0,25 mM EDTA, 0,15
401 mM EGTA, 0,05% NP40, 25% glycerol and protease inhibitors) before centrifugation at 12,000
402 rpm for 5 min at 4ºC to pellet and discard cell debris. The supernatants were used as nuclear
403 fractions.

404 **SIRT1 Activity Assay**

405 NAD^+-dependent deacetylase activity was measured on nuclear extracts of HT-29 cells treated
406 as indicated, using SIRT-Glo Assay kit (Promega), following the manufacturer's instructions.
407 For each reaction, 1 µg of protein was incubated with SIRT-Glo Reagent Mix at room
408 temperature for 3 min, and the luminescence was measured using a GloMax Microplate Reader
409 (Promega). Relative luciferase units (RLU) were calculated as fold induction relative to the
410 corresponding control.

411 **Nuclear NAD^+ abundance**

412 The NAD/NADH-Glo Assay Kit (Promega) was used to measure NAD^+ abundance in HCT 116
413 nuclear extracts. 20 µg of protein were diluted in 50 µl of lysis buffer (described for cell extracts)
414 for each reaction and 25 µl of 0.4 N HCl were added before incubation at 60 °C for 15 minutes.
415 This exploits the high stability of NAD^+ under acidic conditions, while NADH breaks down.
416 Samples were cooled down to room temperature for 10 min and neutralized with 25 µL 0.5 M
417 Trizma®. NAD^+ levels were then measured using a GloMax microplate reader (Promega) and
418 following the manufacturer's instructions.

419 **Immunoprecipitation**

420 For immunoprecipitation from fractionated extracts, the hypotonic buffer was modified by
421 adding 100mM NaCl and 0.1% NP40. For immunocomplex formation, protein A/G-coated
422 magnetic beads (Invitrogen) were washed 3 times with the extraction buffer before coating with
423 the primary antibody for 2 hr at 4 ºC in a rotating wheel, followed by 2 washes with the same

424 buffer to eliminates unbound antibody and then extracts were added O/N at 4ºC in the rotating
425 wheel. Immunocomplexes were washed twice and used for western blotting.

426 **Western blotting**

427 Proteins from lysed cells or immunoprecipitates were denatured and loaded on sodium dodecyl
428 sulfate polyacrylamide gels and then transferred to polyvinylidene difluoride membranes (Bio-
429 Rad). After blocking with 5% (w/v) BSA or milk the membrane was incubated with the
430 corresponding primary and secondary antibodies (Bio-Rad). The specific bands were analyzed
431 using Thyphoon or ChemiDoc Imaging Systems (Bio-Rad).

432 **Immunoflorescence**

433 Cells in cover slips were washed three times and fixed with 4% paraformaldehyde in PBS [pH
434 7.4] for 10min, washed again, permeabilized (PBS [pH7.4], 0.5% Triton X-100, 0.2% BSA) for
435 5min, blocked (PBS [pH7,4, 0,05% Triton X-100, 5% BSA) for 1h at room temperature and
436 incubated with primary antibody over night at 4ºC. After three washes (5 min) cells were
437 incubated with secondary antibody for 1h at room temperature. Slides were mounted and images
438 were acquired using a SP5 confocal microscope (Leica) with a 63x objective. Fluorescence
439 intensity was quantified using Image J software. For each experiment, 3 different fields were
440 evaluated per slide.

441 **Cell-growth curves and cell cycle**

442 Cell growth was determined by colorimetry. For that, cells were seeded at a density of 20,000
443 cells per well in a Corning 12-well plate and treated as indicated for 1 to 6 days. After that cells
444 were treated with 3-(4,5-dimethylthiazol-2-yl)-2,5-diphenyltetrazolium bromide (MTT)
445 (Sigma-.Aldrich) in a 1:10 ratio in a culture medium and incubated at 37 °C for 3 h. In living
446 cells, MTT is reduced to formazan, which has a purple color. The medium was removed, and the
447 formazan was resuspended in dimethylsulfoxide (DMSO), transferred to p96 plates and analyzed
448 by a Spectra FLUOR (Tecan) at 542 nm. Viability was measured in four independent
449 experiments and then duplicated.

450 For cell cycle analysis, cells were harvested by trypsinization, washed with PBS, fixed in 70%
451 ethanol, stained with 7-AAD (Santa Cruz Biotechnology) for 10 min at 37°C, and analyzed by
452 flow cytometry (FACSCalibur, Becton-Dickinson). The percentages of cells at each cell cycle
453 phase were analyzed using CXP software (Becton-Dickinson).

454 **RT-qPCR**

455 Total RNA was extracted from 3 replicates of colorectal cells using TRIzol reagent (Invitrogen).
456 Reverse transcription of 1µg of RNA was performed according to the manufacturer's instructions
457 Reagents and detection systems were from Applied biosystems. 18S ribosomal RNA primers
458 served as a nonregulated control. Relative expression was calculated using the Ct method,
459 expressed as $2^{-\Delta\Delta Ct}$ (Livak and Schmittgen, 2001). The PCR efficiency was approximately
460 100%.

461 **TMA, immunohistochemistry, and quantification.**

462 Tissue microarrays (TMA) containing 92 cores of stage 2 human CRC samples, were constructed
463 using the MTA-1 tissue arrayer (Beecher Instruments, Sun Prairie) for immunohistochemistry
464 analysis. Each core (diameter 0.6 mm) was punched from pre-selected tumour regions in
465 paraffin-embedded tissues. We chose central areas from the tumour, avoiding foci of necrosis.
466 Staining was conducted in 2-µm sections. Slides were deparaffinized by incubation at 60˚C for
467 10 min and incubated with PT-Link (Dako, Agilent) for 20 min at 95˚C in low pH to detect VDR,
468 SIRT1 and acetyl lysines. To block endogenous peroxidase, holders were incubated with
469 peroxidase blocking reagent (Dako, Agilent) and then with (1:50) dilutions of antibodies: anti-
470 VDR, anti-SIRT1 and (1:300) anti-acetyl lysine, overnight at 4˚C. All previously described
471 antibodies presented high specificity. After that, slides were incubated for 20 min with the
472 appropriate anti-Ig horseradish peroxidase-conjugated polymer (EnVision, Dako, Agilent).
473 Sections were then visualized with 3,3'-diaminobenzidine (Dako, Agilent) as a chromogen for 5
474 min and counterstained with Harrys' Haematoxylin (Sigma Aldrich, Merck). Photographs were

475 taken with a stereo microscope (Leica DMi1). According to the human protein atlas (available
476 at http://www.proteinatlas.org), a human colon tissue was used as a positive control for
477 immunohistochemical staining to determine anti-VDR concentration and a human testis tissue
478 for anti-SIRT1. Immunoreactivity was quantified blind with a Histoscore (H score) that considers
479 both the intensity and percentage of cells stained for each intensity (low, medium, or high)
480 following this algorithm (range 0–300): H score = (low%) × 1 + (medium%) × 2 + (high %) ×
481 3. Quantification for each patient biopsy was calculated blindly by 2 investigators (MJFA and
482 JMU). VDR and SIRT1 showed nuclear staining, whereas acetyl lysines were nuclear and
483 extranuclear. Clinicopathological characteristics of patients are summarized in Table 2.

484 **Bioinformatics analyses:**

485 Gene expression (RNA-seq) data from the TCGA colon adenocarcinoma cohort (COAD) was
486 downloaded from the cBioportal for Cancer Genomics (http://www.cbioportal.org) using
487 CGDS-R (Cerami et al., 2012; Gao et al., 2013) following TCGA guidelines
488 (http://cancergenome.nih.gov/publications/publicationguidelines). SIRT1 and VDR gene
489 expression from samples of colorectal cancer and healthy tissue adjacent to the tumour were
490 analysed with TNMplot.com (https://tnmplot.com/analysis/) tool (Bartha and Győrffy, 2021).
491 An asymptotic Spearman correlation test using original log2 expression values was used to
492 determine the significance of the Spearman rank correlation.

493 **Statistical analysis**

494 Results are presented as fold induction, mean ± SEM from three biological replicates. To
495 determine whether calculated Hscores for protein levels were well-modelled by a normal
496 distribution, Kolmogorov-Smirnov test was used. Association between SIRT1 and VDR protein
497 levels was performed with Chi-square test. Comparisons between two independent groups
498 (healthy versus tumors) were performed with Mann-Whitney U-test. For statistical association,
499 Hscore of antigens were categorized as high- or low- expression levels using the median as a

cut-off point. Tests for significance between two sample groups were performed with Student's t test and for multiple comparisons, ANOVA with Bonferroni's post-test.

ACKNOWLEDGMENTS: Funding for this work was provided by the Agencia Estatal de Investigación (PID2019-104867RB-I00 / AEI/10.13039/501100011033, RTI2018-099343-B-100 and PID2021-127645OA-I00); Instituto de Salud Carlos III (CIBERONC, CB16/12/00273 and CB16/12/00326); Comunidad de Madrid (Ayudas Atracción de Talento 2017-T1/BMD-5334 and 2021-5A/BMD-20951; A385-DROPLET Young Reserchers R&D Project 2019 CAM-URJC; PRECICOLON-CM, P2022/BMD7212); Universidad Rey Juan Carlos (ADIPOMELM, Proyecto Puente de Investigación 2020).

We thank Lucille Banham for her valuable assistance in the preparation of the English manuscript and María Gutiérrez Salmerón for help making figures.

Additional Information

FUNDER	GRANT REFERENCE NUMBER	AUTHOR
Agencia Estatal de Investigación	PID2019-110998RB-I00 AEI/10.13039/501100011033	Custodia Garcia-Jimenez
	PID2019-104867RB-I00	Alberto Muñoz & María Jesús Larriba
	RTI2018-099343-B-100	Antonio De la Vieja
	PID2021-127645OA-I00	Ana Chocarro-Calvo
Instituto de Salud Carlos III	CIBERONC CB16/12/00273	Alberto Muñoz
	CIBERONC CB16/12/00326	Antonio De la Vieja
Comunidad de Madrid	PRECICOLON-CM P2022/BMD7212	Custodia García-Jiménez Alberto Muñoz
	Ayudas Atracción de Talento 2017- T1/BMD-5334	Ana Chocarro-Calvo
	Ayudas Atracción de Talento 2021-5A/BMD-20951	
	A385-DROPLET Young Researchers R&D Project 2019	
Universidad Rey Juan Carlos	ADIPOMELM, Proyecto Puente de Investigación 2020	

The funders had no role in study design, data collection and interpretation, or the decision to submit the work for publication

515

516 **Author contributions:** CGJ, JMGM, AM, and MJL conceived the experiments, JMGM, ACC,
517 AB, JMU, MJFA, MCF, JCR performed the experiments. JMGM and ADLV performed the Figs.
518 All authors participated in the discussion. CGJ, AM and MJL wrote the manuscript and provided
519 supervision.

520

521 **Ethics**

522 The authors declare that they have no conflict of interest. All procedures followed were in
523 accordance with the ethical standards of the responsible committee on human experimentation
524 (institutional and national) as specified under the paragraph Human samples in the Materials and
525 Methods Section and with the Helsinki Declaration of 1975, as revised in 2000. lnformed consent
526 was obtained from all patients for being included in the study.

527

528 **REFERENCES**

529 An B-S, Tavera-Mendoza LE, Dimitrov V, Wang X, Calderon MR, Wang H-J, White JH.
530 2010. Stimulation of Sirt1-Regulated FoxO Protein Function by the Ligand-Bound
531 Vitamin D Receptor. *Mol Cell Biol* **30**:4890–4900. doi:10.1128/MCB.00180-10

532 Bartha Á, Győrffy B. 2021. Tnmplot.Com: A web tool for the comparison of gene expression
533 in normal, tumor and metastatic tissues. *Int J Mol Sci* **22**:1–12.
534 doi:10.3390/ijms22052622

535 Bikle D, Christakos S. 2020. New aspects of vitamin D metabolism and action — addressing
536 the skin as source and target. *Nat Rev Endocrinol* **16**:234–252. doi:10.1038/s41574-
537 019-0312-5

538 Bonkowski MS, Sinclair DA. 2016. Slowing ageing by design: The rise of NAD+ and
539 sirtuin-activating compounds. *Nat Rev Mol Cell Biol* **17**:679–690.
540 doi:10.1038/NRM.2016.93

541 Cancer Genome Atlas Network. 2012. Comprehensive molecular characterization of human
542 colon and rectal cancer. *Nature* **487**:330–337. doi:10.1038/nature11252

543 Carafa V, Altucci L, Nebbioso A. 2019. Dual Tumor Suppressor and Tumor Promoter
544 Action of Sirtuins in Determining Malignant Phenotype. *Front Pharmacol* **10**:38.
545 doi:10.3389/fphar.2019.00038

546 Carlberg C, Muñoz A. 2022. An update on vitamin D signaling and cancer. *Semin Cancer*
547 *Biol* **79**:217–230. doi:10.1016/j.semcancer.2020.05.018

548 Carlberg C, Velleuer E. 2022. Vitamin D and the risk for cancer: A molecular analysis.
549 *Biochem Pharmacol* **196**. doi:10.1016/J.BCP.2021.114735

550 Cerami E, Gao J, Dogrusoz U, Gross BE, Sumer SO, Aksoy BA, Jacobsen A, Byrne CJ,
551 Heuer ML, Larsson E, Antipin Y, Reva B, Goldberg AP, Sander C, Schultz N. 2012.
552 The cBio Cancer Genomics Portal: An open platform for exploring multidimensional
553 cancer genomics data. *Cancer Discov* **2**:401–404. doi:10.1158/2159-8290.CD-12-0095

554 Chandler PD, Chen WY, Ajala ON, Hazra A, Cook N, Bubes V, Lee I-M, Giovannucci EL,
555 Willett W, Buring JE, Manson JE. 2020. Effect of Vitamin D $_3$ Supplements on
556 Development of Advanced Cancer. *JAMA Netw Open* **3**:e2025850.
557 doi:10.1001/jamanetworkopen.2020.25850

558 Chen X, Sun K, Jiao S, Cai N, Zhao X, Zou H, Xie Y, Wang Z, Zhong M, Wei L. 2014.
559 High levels of SIRT1 expression enhance tumorigenesis and associate with a poor
560 prognosis of colorectal carcinoma patients. *Sci Rep* **4**. doi:10.1038/SREP07481

561 Chocarro-Calvo A, García-Martínez JM, Ardila-González S, de la Vieja A, García-Jiménez
562 C. 2013. Glucose-Induced β-Catenin Acetylation Enhances Wnt Signaling in Cancer.
563 *Mol Cell* **49**:474–486. doi:10.1016/j.molcel.2012.11.022

564 Evans SR, Nolla J, Hanfelt J, Shabahang M, Nauta RJ, Shchepotin IB. 1998. Vitamin D
565 receptor expression as a predictive marker of biological behavior in human colorectal
566 cancer. *Clinical Cancer Research* **4**:1591–1595.

567 Bray F., Ferlay J., Soerjomataram I, Siegel RL, Torre LA, Jemal A. 2018. Global cancer
568 statistics 2018: GLOBOCAN estimates of incidence and mortality worldwide for 36
569 cancers in 185 countries. *CA Cancer J Clin* **68**:394–424. doi:10.3322/caac.21492

570 Fang J, Ianni A, Smolka C, Vakhrusheva O, Nolte H, Krüger M, Wietelmann A, Simonet
571 NG, Adrian-Segarra JM, Vaquero A, Braun T, Bober E. 2017. Sirt7 promotes
572 adipogenesis in the mouse by inhibiting autocatalytic activation of Sirt1. *Proc Natl*
573 *Acad Sci U S A* **114**:E8352–E8361. doi:10.1073/pnas.1706945114

574 Feldman D, Krishnan A V., Swami S, Giovannucci E, Feldman BJ. 2014. The role of vitamin
575 D in reducing cancer risk and progression. *Nat Rev Cancer*. doi:10.1038/nrc3691

576 Fernández-Barral A, Bustamante-Madrid P, Ferrer-Mayorga G, Barbáchano A, Larriba MJ,
577 Muñoz A. 2020. Vitamin D Effects on Cell Differentiation and Stemness in Cancer.
578 *Cancers (Basel)* **12**:2413–2432. doi:10.3390/cancers12092413

579 Ferrer-Mayorga G, Gómez-López G, Barbáchano A, Fernández-Barral A, Peña C, Pisano
580 DG, Cantero R, Rojo F, Muñoz A, Larriba MJ. 2017. Vitamin D receptor expression
581 and associated gene signature in tumour stromal fibroblasts predict clinical outcome in
582 colorectal cancer. *Gut* **66**:1449–1462. doi:10.1136/gutjnl-2015-310977

583 Ferrer-Mayorga G, Larriba MJ, Crespo P, Muñoz A. 2019. Mechanisms of action of vitamin
584 D in colon cancer. *J Steroid Biochem Mol Biol* **185**:1–6.
585 doi:10.1016/j.jsbmb.2018.07.002

586 Firestein R, Blander G, Michan S, Oberdoerffer P, Ogino S, Campbell J, Bhimavarapu A,
587 Luikenhuis S, de Cabo R, Fuchs C, Hahn WC, Guarente LP, Sinclair DA. 2008. The
588 SIRT1 Deacetylase Suppresses Intestinal Tumorigenesis and Colon Cancer Growth.
589 *PLoS One* **3**:e2020. doi:10.1371/journal.pone.0002020

590 Gao J, Aksoy BA, Dogrusoz U, Dresdner G, Gross B, Sumer SO, Sun Y, Jacobsen A, Sinha
591 R, Larsson E, Cerami E, Sander C, Schultz N. 2013. Integrative analysis of complex
592 cancer genomics and clinical profiles using the cBioPortal. *Sci Signal* **6**:1–34.
593 doi:10.1126/scisignal.2004088

594 Giardina C, Nakanishi M, Khan A, Kuratnik A, Xu W, Brenner B, Rosenberg DW. 2015.
595 Regulation of VDR expression in Apc-mutant mice, human colon cancers and
596 adenomas. *Cancer Prevention Research* **8**:387–399. doi:10.1158/1940-6207.CAPR-
597 14-0371

598 Grant WB, Boucher BJ, al Anouti F, Pilz S. 2022. Comparing the Evidence from
599 Observational Studies and Randomized Controlled Trials for Nonskeletal Health
600 Effects of Vitamin D. *Nutrients* **14**:1–31.

601 Gutiérrez-Salmerón M, García-Martínez JM, Martínez-Useros J, Fernández-Aceñero MJ,
602 Viollet B, Olivier S, Chauhan J, Lucena SR, de la Vieja A, Goding CR, Chocarro-Calvo
603 A, García-Jiménez C. 2020. Paradoxical activation of AMPK by glucose drives
604 selective EP300 activity in colorectal cancer. *PLoS Biol* **18**:e3000732.
605 doi:10.1371/journal.pbio.3000732

606 Han Y, Jin YH, Kim YJ, Kang BY, Choi HJ, Kim DW, Yeo CY, Lee KY. 2008. Acetylation
607 of Sirt2 by p300 attenuates its deacetylase activity. *Biochem Biophys Res Commun*
608 **375**:576–580. doi:10.1016/j.bbrc.2008.08.042

609 Henn M, Martin-Gorgojo V, Martin-Moreno JM. 2022. Vitamin D in Cancer Prevention:
610 Gaps in Current Knowledge and Room for Hope. *Nutrients* **14**:1–32.

611 Kim H, Lipsyc-Sharf M, Zong X, Wang X, Hur J, Song M, Wang M, Smith-Warner SA,
612 Fuchs C, Ogino S, Wu K, Chan AT, Cao Y, Ng K, Giovannucci EL. 2021. Total
613 Vitamin D Intake and Risks of Early-Onset Colorectal Cancer and Precursors.
614 *Gastroenterology* **161**:1208-1217.e9. doi:10.1053/j.gastro.2021.07.002

615 Kim H, Yuan C, Nguyen LH, Ng K, Giovannucci EL. 2022. Prediagnostic Vitamin D Status
616 and Colorectal Cancer Survival by Vitamin D Binding Protein Isoforms in US Cohorts.
617 *J Clin Endocrinol Metab*. doi:10.1210/CLINEM/DGAC742

618 Larriba MJ, González-Sancho JM, Barbáchano A, Niell N, Ferrer-Mayorga G, Muñoz A.
619 2013. Vitamin D is a multilevel repressor of Wnt/β-catenin signaling in cancer cells.
620 *Cancers (Basel)*. doi:10.3390/cancers5041242

621 Larriba MJ, Martín-Villar E, García JM, Pereira F, Peña C, García de Herreros A, Bonilla F,
622 Muñoz A. 2009. Snail2 cooperates with Snail1 in the repression of vitamin D receptor
623 in colon cancer. *Carcinogenesis* **30**. doi:10.1093/carcin/bgp140

624 Larriba MJ, Muñoz A. 2005. SNAIL vs vitamin D receptor expression in colon cancer:
625 therapeutics implications. *Br J Cancer* **92**:985–989. doi:10.1038/sj.bjc.6602484

626 Larriba MJ, Ordóñez-Morán P, Chicote I, Martín-Fernández G, Puig I, Muñoz A, Pálmer
627 HG. 2011. Vitamin D receptor deficiency enhances Wnt/β-catenin signaling and tumor
628 burden in colon cancer. *PLoS One* **6**:e23524. doi:10.1371/journal.pone.0023524

629 Livak KJ, Schmittgen TD. 2001. Analysis of relative gene expression data using real-time
630 quantitative PCR and the 2(-Delta Delta C(T)) Method. *Methods* **25**:402–408.
631 doi:10.1006/meth.2001.1262

632 Manson JE, Bassuk SS, Buring JE, VITAL Research Group. 2020. Principal results of the
633 VITamin D and OmegA-3 TriaL (VITAL) and updated meta-analyses of relevant
634 vitamin D trials. *J Steroid Biochem Mol Biol* **198**:105522.
635 doi:10.1016/j.jsbmb.2019.105522

636 Mendes KL, Lelis D de F, Santos SHS. 2017. Nuclear sirtuins and inflammatory signaling
637 pathways. *Cytokine Growth Factor Rev* **38**:98–105. doi:10.1016/j.cytogfr.2017.11.001

638 Muñoz A, Grant WB. 2022. Vitamin D and Cancer: An Historical Overview of the
639 Epidemiology and Mechanisms. *Overview of the Epidemiology and Mechanisms*
640 *Nutrients* **14**:1448. doi:10.3390/nu14071448

641 Oppenheimer H, Gabay O, Meir H, Haze A, Kandel L, Liebergall M, Gagarina V, Lee EJ,
642 Dvir-Ginzberg M. 2012. 75-kd sirtuin 1 blocks tumor necrosis factor α-mediated
643 apoptosis in human osteoarthritic chondrocytes. *Arthritis Rheum* **64**:718–728.
644 doi:10.1002/ART.33407

645 Pálmer HG, Larriba MJ, García JM, Ordóñez-Morán P, Peña C, Peiró S, Puig I, Rodríguez
646 R, de La Fuente R, Bernad A, Pollán M, Bonilla F, Gamallo C, García De Herreros A,
647 Muñoz A. 2004. The transcription factor SNAIL represses vitamin D receptor
648 expression and responsiveness in human colon cancer. *Nat Med* **10**:917–919.
649 doi:10.1038/nm1095

650 Patel KR, Scott E, Brown VA, Gescher AJ, Steward WP, Brown K. 2011. Clinical trials of
651 resveratrol. *Ann N Y Acad Sci* **1215**:161–169. doi:10.1111/j.1749-6632.2010.05853.x

652 Peña C, Garciá JM, Silva J, García V, Rodríguez R, Alonso I, Millán I, Salas C, García de
653 Herreros A, Muñoz A, Bonilla F. 2005. E-cadherin and vitamin D receptor regulation
654 by SNAIL and ZEB1 in colon cancer: Clinicopathological correlations. *Hum Mol Genet*
655 **14**:3361–3370. doi:10.1093/hmg/ddi366

656 Polidoro L, Properzi G, Marampon F, Gravina GL, Festuccia C, di Cesare E, Scarsella L,
657 Ciccarelli C, Zani BM, Ferri C. 2013. Vitamin D protects human endothelial cells from
658 H2O2 oxidant injury through the Mek/Erk-sirt1 axis activation. *J Cardiovasc Transl*
659 *Res* **6**:221–231. doi:10.1007/s12265-012-9436-x

660 Ren NSX, Ji M, Tokar EJ, Busch EL, Xu X, Lewis DA, Li Xiangchun, Jin A, Zhang Y, Wu
661 WKK, Huang W, Li L, Fargo DC, Keku TO, Sandler RS, Li Xiaoling. 2017.
662 Haploinsufficiency of SIRT1 Enhances Glutamine Metabolism and Promotes Cancer
663 Development. *Current Biology* **27**:483–494. doi:10.1016/j.cub.2016.12.047

664 Sabir MS, Khan Z, Hu C, Galligan MA, Dussik CM, Mallick S, Stone AD, Batie SF, Jacobs
665 ET, Whitfield GK, Haussler MR, Heck MC, Jurutka PW. 2017. SIRT1 enzymatically

666 potentiates 1,25-dihydroxyvitamin D3 signaling via vitamin D receptor deacetylation.
667 *J Steroid Biochem Mol Biol* **172**:117–129. doi:10.1016/J.JSBMB.2017.06.010

668 Song M, Lee IM, Manson JAE, Buring JE, Dushkes R, Gordon D, Walter J, Wu K, Chan
669 AT, Ogino S, Fuchs CS, Meyerhardt JA, Giovannucci EL. 2021. No Association
670 Between Vitamin D Supplementation and Risk of Colorectal Adenomas or Serrated
671 Polyps in a Randomized Trial. *Clinical Gastroenterology and Hepatology* **19**:128-
672 135.e6. doi:10.1016/j.cgh.2020.02.013

673 Strycharz J, Rygielska Z, Swiderska E, Drzewoski J, Szemraj J, Szmigiero L, Sliwinska A.
674 2018. SIRT1 as a Therapeutic Target in Diabetic Complications. *Curr Med Chem*
675 **25**:1002–1035. doi:10.2174/0929867324666171107103114

676 Vaziri H, Dessain SK, Eaton EN, Imai SI, Frye RA, Pandita TK, Guarente L, Weinberg RA.
677 2001. hSIR2SIRT1 functions as an NAD-dependent p53 deacetylase. *Cell* **107**:149–
678 159. doi:10.1016/S0092-8674(01)00527-X

679 Wang L, Du Y, Lu M, Li T. 2012. ASEB: a web server for KAT-specific acetylation site
680 prediction. *Nucleic Acids Res* **40**:W376–W379. doi:10.1093/nar/gks437

681 Wu S, Jiang J, Liu J, Wang X, Gan Y, Tang Y. 2017. Meta-analysis of SIRT1 expression as
682 a prognostic marker for overall survival in gastrointestinal cancer. *Oncotarget* **8**:62589–
683 62599. doi:10.18632/oncotarget.19880

684 Yousafzai NA, Jin H, Ullah M, Wang X. 2021. Recent advances of SIRT1 and implications
685 in chemotherapeutics resistance in cancer. *Am J Cancer Res* **Nov 15**:5233-5248.

686 Yuan Q, Zhang R, Sun M, Guo X, Yang J, Bian W, Xie C, Miao D, Mao L. 2022. Sirt1
687 Mediates Vitamin D Deficiency-Driven Gluconeogenesis in the Liver via mTorc2/Akt
688 Signaling. doi:10.1155/2022/1755563

689 Zheng W, Wong KE, Zhang Z, Dougherty U, Mustafi R, Kong J, Deb DK, Zheng H,
690 Bissonnette M, Li YC. 2012. Inactivation of the vitamin D receptor in APC(min/+)
691 mice reveals a critical role for the vitamin D receptor in intestinal tumor growth. *Int J*
692 *Cancer* **130**:10–19. doi:10.1002/IJC.25992

693

694

695 **FIGURE LEGENDS**

696 **Fig. 1.** ***1,25(OH)$_2$D$_3$ increases SIRT1 levels in CRC cells and VDR is required to ensure basal***
697 ***levels.***

698 (A)-(D) HCT 116 or HT-29 CRC cells cultured under standard conditions and where indicated,
699 treated with 1α,25-dihydroxyvitamin D$_3$ (1,25(OH)$_2$D$_3$), 100 nM, added 24 hours before
700 harvesting. (E)-(H) ShVDR cells were derived from HCT 116 by stable and specific knock-down

701 of vitamin D receptor (VDR) using specific shRNA and are compared to ShControl cells that
702 contain normal VDR levels (Larriba et al., 2011). Cell extracts were fractionated in all cases.

703 (A) Confocal imaging of SIRT1 (green) in CRC (HCT 116 and HT-29) cells and fluorescence
704 intensity quantification of 3 independent experiments using ImageJ software. For each
705 experiment 3 different fields were evaluated per slide. Scale bars:25µm.

706 (B) Western-blot analysis of 1,25$(OH)_2D_3$ effects on levels of SIRT1 in nuclear extracts (NE)
707 from indicated CRC cells. Representative blots and statistical analysis using TBP as loading
708 controls.

709 (C)-(E) RT-qPCR analysis of the effect of 1,25 $(OH)_2D_3$ in indicated colon cancer cells. Values
710 normalized with endogenous control (18S RNA) are referred as fold induction over cells without
711 1,25$(OH)_2D_3$.
712 (C) Effect of 1,25 $(OH)_2D_3$ on SIRT1 gene expression.
713 (D) validation of 1,25 $(OH)_2D_3$ activity on the canonical target gene cytochrome P450 family 24
714 subfamily A member 1, CYP24A1, in HT-29 colon cancer cells.
715 (E) Requirement of vitamin D receptor (VDR) for 1,25 $(OH)_2D_3$ induction of SIRT1 gene
716 expression.
717 (F) Effect of VDR knock-down on SIRT1 protein content evaluated by confocal imaging of
718 ShControl and ShVDR HCT 116 colon cancer cells to detect SIRT1 (green). Scale bars represent
719 25 µm. On the right, quantification of fluorescence intensity using ImageJ software; for each
720 experiment, 3 different fields were evaluated per slide.
721 (G) Western blot analysis of the effect of 1,25 $(OH)_2D_3$ on nuclear accumulation of SIRT1 in
722 cells depleted (ShVDR) or not (ShControl) of VDR.
723 (H) Specificity of 1,25 $(OH)_2D_3$ effects on SIRT1 by western blot analysis of the alternative
724 nuclear sirtuin, SIRT7.

725 Statistical analysis of 3 independent experiments in each panel was performed by Student t-test
726 (A) to (D) and (H) or by One-Way ANOVA (E)-(F). For (G), statistical analysis of the four
727 groups by ANOVA is represented by * and comparison of the two indicated groups by Students
728 t test, by #. In all panels, values represent mean ± SEM of triplicates corresponding to biological
729 replicates; * or # $p< 0.05$; ** $p< 0.01$; *** $p< 0.001$.

730 **Fig. 2.** ***1,25(OH)$_2$D$_3$ induces specific SIRT1 deacetylase activity independently of levels, in***
731 ***CRC cells.***

732 Cells were cultured as in Fig 1.

733 (A) and (G) NAD^+-dependent deacetylase activity, (B) Evaluation of nuclear NAD^+ levels. (C)
734 to (F) Western blot analysis using TBP or H3 as loading controls. Representative western blots
735 and statistical analysis of 3 independent experiments.

736 (A) NAD^+-dependent deacetylase activity measured on nuclear extracts of HT-29 cells. Relative
737 luciferase units (RLU) were calculated as fold induction relative to the corresponding control.

738 (B) Evaluation of nuclear NAD^+ levels in HT-29 CRC cells in response to 1,25(OH)$_2$D$_3$, with
739 data expressed as fold induction over the control, untreated cells.

740 (C) 1,25(OH)$_2$D$_3$ effects on the interaction between vitamin D receptor (VDR) and SIRT1. Input
741 (5%) and flow through (FT) are shown

742 (D) 1,25(OH)$_2$D$_3$ effects on the acetylation status of the SIRT1 substrate FoxO3a in nuclear
743 extracts immunoprecipitated with anti-acetyl lysine antibodies. Input (5%) and flow through
744 (FT) are shown.

745 (E) 1,25(OH)$_2$D$_3$ effects on the nuclear acetylation of the SIRT1 substrate H3K9 (Ace H3K9).

746 (F) Requirement of VDR for deacetylation of Ace H3K9 in response to 1,25(OH)$_2$D$_3$

747 (G) Quantification of NAD^+-dependent deacetylase activity on SIRT1 immunoprecipitates from
748 nuclear extracts (NE) of HCT 116 CRC cells treated or not with $1,25(OH)_2D_3$. Values represent
749 mean ± SEM of n=3 independent experiments.

750 Statistical analysis by Student t test, n ≥ 3 biological replicates and values represent mean ±
751 SEM; *p<0.05; **p<0.01; *** p<0.001.

752 **Fig. 3.** ***CRC biopsies exhibit discrepancies between SIRT1 protein levels and deacetylase***
753 ***activity***

754 (A)-(B) TNM plot analysis of VDR (A) or SIRT1 (B) gene expression in 160 paired samples of
755 non-cancer adjacent tissue (normal) versus adenocarcinoma tissue (tumour). Data was collected
756 from TCGA-COAD database. SIRT1 or VDR expression is shown as transcripts per million
757 (TPM) in log2. Tumour and control samples were compared with Mann-Whitney U test. The
758 statistical significance cut off was set at $p < 0.01$.

759 (C) Association analysis between VDR and SIRT1 protein levels in human colon cancer samples,
760 stage 2. Cut-off points to separate proteins between high- or low- expression levels were for
761 SIRT1 expression median of Histoscore, and negative *versus* positive staining for VDR
762 expression. Statistical analysis was performed with Chi-square test.

763 (D) Representative micrographs at 40X from immunostaining for vitamin D receptor (VDR) or SIRT1
764 on human samples of healthy colon or CRC patients. Scale bars: 20µm. Immunostainings were
765 revealed with DAB (diaminebenzidine) and thus, positiveness is highlighted by light or dark brown
766 according to their low or high protein expression. Counterstaining with hematoxilin stains nuclei
767 in dark blue and cytoplasm in light blue.

768 (E) Profile for SIRT1 content from healthy to colon cancer human samples. The profile was
769 obtained from Histoscore variations. Tumour and control samples were compared with Mann-
770 Whitney U test. The statistical significance cut off was set at $p < 0.01$.

771 (F) Western-blot analysis of the levels of SIRT1 and its substrate Ace H3K9 in total lysates from
772 intestinal healthy (HIEC6) or CRC cells. Representative western blot with ERK as loading
773 control.

774 (G) Western-blot analysis from human patient samples, with patient number indicated at the top.
775 CRC samples (T) and adjacent nontumor tissue (NT) were probed for SIRT1 and its substrate
776 Ace H3K9 (as in F). Frozen samples were obtained from HUFA patients.

777 (H) NAD^+-dependent deacetylase activity on immunoprecipitated SIRT1 from patient lysates.
778 Values for T and NT samples were corrected according to immunoprecipitated SIRT1 levels
779 shown on the western underneath the graph. Values for T samples were referred to values of NT
780 and data (duplicates) are expressed as fold induction. Patient number is indicated at the bottom.

781 (I) Western-blot analysis for SIRT1 and its substrate Ace H3K9 levels in total lysates from
782 alternative human CRC samples (as in G). Patient number is indicated at the top.

783 (J) NAD^+-dependent deacetylase activity on immunoprecipitated SIRT1 from patient lysates
784 presented in (I). Levels of immunoprecipitated SIRT1 are presented in the bottom panel. SIRT1
785 deacetylase activity in patients is presented as fold induction, referred to the first patient sample
786 (patient #10). Patient number is indicated at the bottom.

787

788 **Fig. 4.** ***1,25(OH)$_2$D$_3$ induces SIRT1 activity through auto deacetylation***

789 HCT 116 CRC cells were cultured under standard conditions in DMEM containing LiCl (40
790 mM) to mimic Wnt signalling before addition of 1,25(OH)$_2$D$_3$, 100 nM or SRT1720 (20 μM)
791 for the last 24 h; after fractionation nuclear extracts (NE) were used. (A)-(C) and (E)-(F)
792 Immunoprecipitation (IP) using anti-acetyl lysine antibody from nuclear extracts (NE) of
793 indicated cells and western-blot analysis to evaluate changes in acetylation of SIRT1; TBP was

794 used in the Flow Through (FT) as loading control. Representative western-blots and statistical
795 analysis are shown in all panels.

796 (A) Effect of 1,25$(OH)_2D_3$ on acetylation of SIRT1.

797 (B) Effect of SRT1720 on acetylation of SIRT1. (C) Requirement of VDR for 1,25(OH)2D_3 or
798 SRT1720 effects on acetylation of SIRT1 in Sh Control and ShVDR HCT 116 cells.

799 (D) SIRT1 scheme with functional domains and putative acetylation sites (top) and sequence
800 alignment. Conserved putative acetylation targets for activation/inactivation of SIRT1 shown at
801 the bottom.

802 (E) Acetylation status of exogenous SIRT1 wild type (WT) or mutants (H363Y or K610R). HCT
803 116 were transiently transfected with pcDNA expression vectors: empty (-), myc-tagged SIRT1
804 wild type (WT) or mutants: H363Y inactive or K610R, 48 h before harvesting.
805 Immunoprecipitation using anti-acetyl-lysine antibodies and western blot detection using myc
806 antibodies. Representative western-blot and statistical analysis; MYC and TBP in the flow
807 through (FT) serve as loading controls.

808 (F) Western-blot analysis of the interaction of SIRT1 wild type and mutants, with vitamin D
809 receptor (VDR). Expression and analysis as in (E).

810 (G) Western-blot analysis of the effect of SIRT1 mutant expression on Ace H3K9.

811 (H) *In vitro* NAD^+-dependent deacetylase activity assays on equivalent amounts of exogenous
812 SIRT1 wild type (WT), K610R and inactive H363Y mutants immunoprecipitated using anti-myc
813 antibodies.

814 Statistical analysis in all panels except (D) and (G) by One Way ANOVA of n>3 independent
815 experiments. Values represent mean ± SEM; *p<0.05; **p<0.01; *** p<0.001.

816 **Fig. 5.** ***SIRT1 activation rescues antiproliferative effects of*** 1,25$(OH)_2D_3$ ***in unresponsive CRC***
817 ***cells.***

818 Cells were cultured as in previous figures and treatments with NAA (300 uM), SRT1720 (20μM)
819 and 1,25 $(OH)_2D_3$ (100 nM) also were for the last 24 h.

820 (A) Flow cytometry analysis of cell cycle from indicated cells treated (+) or not (-) with
821 1,25$(OH)_2D_3$. Numbers correspond to the percentage of cells in the indicated phases expressed
822 as mean ± SEM.

823 (B) Effect of NAA on the 1,25$(OH)_2D_3$-driven blockades of HCT 116 CRC cell proliferation.

824 (C) Effects of SRT1720 on cell cycle of HCT 116 CRC cells by flow cytometry analysis.
825 Numbers correspond to the percentage of cells in the indicated phases expressed as mean ± SEM.

826 (D) Flow cytometry analysis of cell cycle response to 1,25 $(OH)_2D_3$ in ShControl and ShVDR
827 HCT 116 cells. Numbers correspond to the percentage of cells in the indicated phases expressed
828 as mean ± SEM.

829 (E) Proliferation curves of ShControl or ShVDR HCT 116 colon cancer cells in response to 1,25
830 $(OH)_2D_3$ (100 nM) (grey), compared to control with vehicle (green) or SRT1720 (red).
831 Statistical analysis by One-Way ANOVA of 3 independent experiments; values represent
832 mean ± SEM of triplicates; * $p< 0.05$; ** $p< 0.01$; *** $p< 0.001$.

833

Table 1. Key Materials & Resources.

Antibodies		
Rabbit Polyclonal anti-Acetylated-lysine	Cell Signaling	Cat# 9441
Rabbit monoclonal anti-Histone H3K9-Ace (C5B11)		Cat # 9649
Rabbit Polyclonal anti-Histone H3		Cat # 9715
Rabbit Polyclonal anti-Vitamin D3 receptor (D2K6W)		Cat #12550
Rabbit monoclonal anti-FoxO3a (75D8)		Cat# 2497
Rabbit Polyclonal anti-SIRT1 (D1D7)		Cat# 9475
Rabbit Polyclonal anti-SIRT1	Santa Cruz Biotechnology	Cat#SC-15404
Rabbit Polyclonal anti-TFIID-TBP (N12)		Cat# SC-204
Rabbit Polyclonal anti-SIRT7		Cat#SC365344
Rabbit Polyclonal anti-ERK (C14)		Cat# SC-154
Mouse Monoclonal anti-MYC (9E10)		Cat# SC-40
Donkey Anti-Rabbit-AlexaFluor488	Invitrogen	Cat# A21206
Mouse monoclonal anti-TBP (51841)		Cat# MA514739
Goat Anti-Rabbit IgG (H+L) HRPO	BIO-RAD	Cat #170-6515
Goat Anti-Mouse IgG (H+L) HRPO		Cat #170-6516
Mouse Monoclonal anti-Tubulin Clone B-5-1-2	Sigma-Aldrich	Cat# T5168
EnVision + Dual Link System-HRP (DAB+)	Dako (Agilent)	Cat#K4065
Chemicals, Peptides, and Recombinant Proteins		
1α,25-DihydroxyVD$_3$	Sigma-Aldrich	17936
Lithium Chloride	Sigma-Aldrich	Cat# L9650
BSA	Sigma-Aldrich	A7906
Nicotinamide (NAA)	Sigma-Aldrich	N3376
SRT1720	Selleckchem	S1129
TRIzol reagent	Invitrogen	Cat#15596026
Protease inhibitor Cocktail	Roche	Cat#04693132001
7-AAD	Santa Cruz Biotechnology	SC-221210

3-(4,5-dimetiltiazol-2-il)-2,5-difeniltetrazol (MTT)	Sigma-Aldrich	Cat# M5655
DMEM media	Lonza	Cat# 12-604F
Bovine Fetal Serum	Sigma	Cat# F7524
JetPEI PolyPlus reagent	Genycell Biotech	Cat# 101-10N
JetPRIME PolyPlus reagent	Genycell Biotech	Cat # 114-01
QuickChange Site-Directed Mutagenesis Kit	Stratagene	Cat #200523
SIRT-Glo Assay kit	Promega	G6450
NAD/NADH-Glo Assay Kit	Promega	G9071
DYNAbeads Protein A	Invitrogen	Ref 10002D
DYNAbeads Protein G	Invitrogen	Ref 10004D
Bacterial Strains		
E. coli 5α	New England Biolabs	NEB5α
Experimental Models: Cell Lines		
HCT 116 (Male) colorectal carcinoma	ATCC	Cat# CCL-247, RRID:CVCL_0291
HT-29 (Female). Rectosigmoid adenocarcinoma	ATCC	Cat# HTB-38, RRID:CVCL_0320
HCT 116 ShControl	In house	(Larriba et al. 2011)
HCT 116 ShVDR	In house	(Larriba et al. 2011)
Oligonucleotides		
Human SIRT1 K610R mutagenesis primers F 5′-3′: GGTTCTAGTACTGGGGAGAGGAATGAAAGAACTTCAGTGG R 5′-3′: CCAGCCACTGAAGTTCTTTCATTCCTCTCCCCAGTACTAG	Sigma	This study
Human CYCLIN D1 (CCND1) qPCR primers F 5′-3′: AAGATCGTCGCCACCTGG R 5′-3′: GGAAGACCTCCTCCTCGCAC	Sigma	This study
Human c-MYC qPCR primers F 5′-3′: CTTCTCTCCGTCCTCGGATTCT R 5′-3′: GAAGGTGATCCAGACTCTGACCTT	Sigma	This study
Human 18s qPCR primers F 5′-3′: AGTCCCTGCCCTTTGTACACA R 5′-3′ GCCTCACTAAACCATCCAATCG	Sigma	This study
CYP24A1 TaqMan® probe	Applied Biosystems	Hs00167999_m1
Recombinant DNA		
pcDNA3.1-SIRT1-Myc-His	Gift from Prof. Colin R Goding	N/A
pcDNA3.1-SIRT1H363Y- Myc-His	Gift from Prof. Colin R Goding	N/A
pcDNA3.1-SIRT1 K601R- Myc-His	This study	N/A
Software and Algorithms		
LAS AF software	Leica	SP5
3730xl Analyzer	Applied Biosystem	ABI 3730XL
GraphPad Prism software	GraphPad Software	https://www.graphpad.com

ImageLab	Bio-Rad	ChemiDoc XRS+ System
CXP software	Becton-Dickinson	FACSCalibur
ImageJ software	https://imagej.nih.gov/ij/download.html	N/A
SPSS Statistics version 26	IBM	N/A

Table 2. Clinicopathological characteristics of CRC patients included in the study.

Patients Characteristic	N (%)	
	Stage II	Stage IV
Gender		
Male	57 (60%)	27 (48%)
Female	38 (40%)	23 (41%)
N/A	0	6 (11%)
Tumor Location		
Cecum	13 (14%)	3 (5%)
Right	25 (26%)	10 (18%)
Transverse	7 (8%)	3 (5%)
Left	5 (5%)	2 (4%)
Sigma	24 (25%)	21 (38%)
Rectum	21 (21%)	12 (21%)
N/A	0	5 (9%)
Grade Primary Tumor		
Well differentiated	18 (19%)	15 (27%)
Moderately differentiated	69 (73%)	27 (48%)
Poorly differentiated	8 (8%)	5 (9%)
N/A	0	9 (16%)
Paired Liver Metastasis		54 (96%)
N/A		2 (4%)
Grade Metastasis Tumor		
Well differentiated		12 (21%)
Moderately differentiated		29 (52%)
Poorly differentiated		4 (7%)
N/A		11 (20%)
Metastasis at diagnosis		
Synchronous		35 (62%)
Metachronous		21 (38%)
Pt		
T1	3 (3%)	2 (4%)
T2	30 (32%)	5 (9%)
T3	61 (64%)	42 (75%)
T4	1 (1%)	4 (7%)
N/A		3 (5%)
pN		
N0	95 (100%)	27 (48%)
N1		16 (29%)
N2		9 (16%)
N3		1 (2%)
N/A		3 (5%)

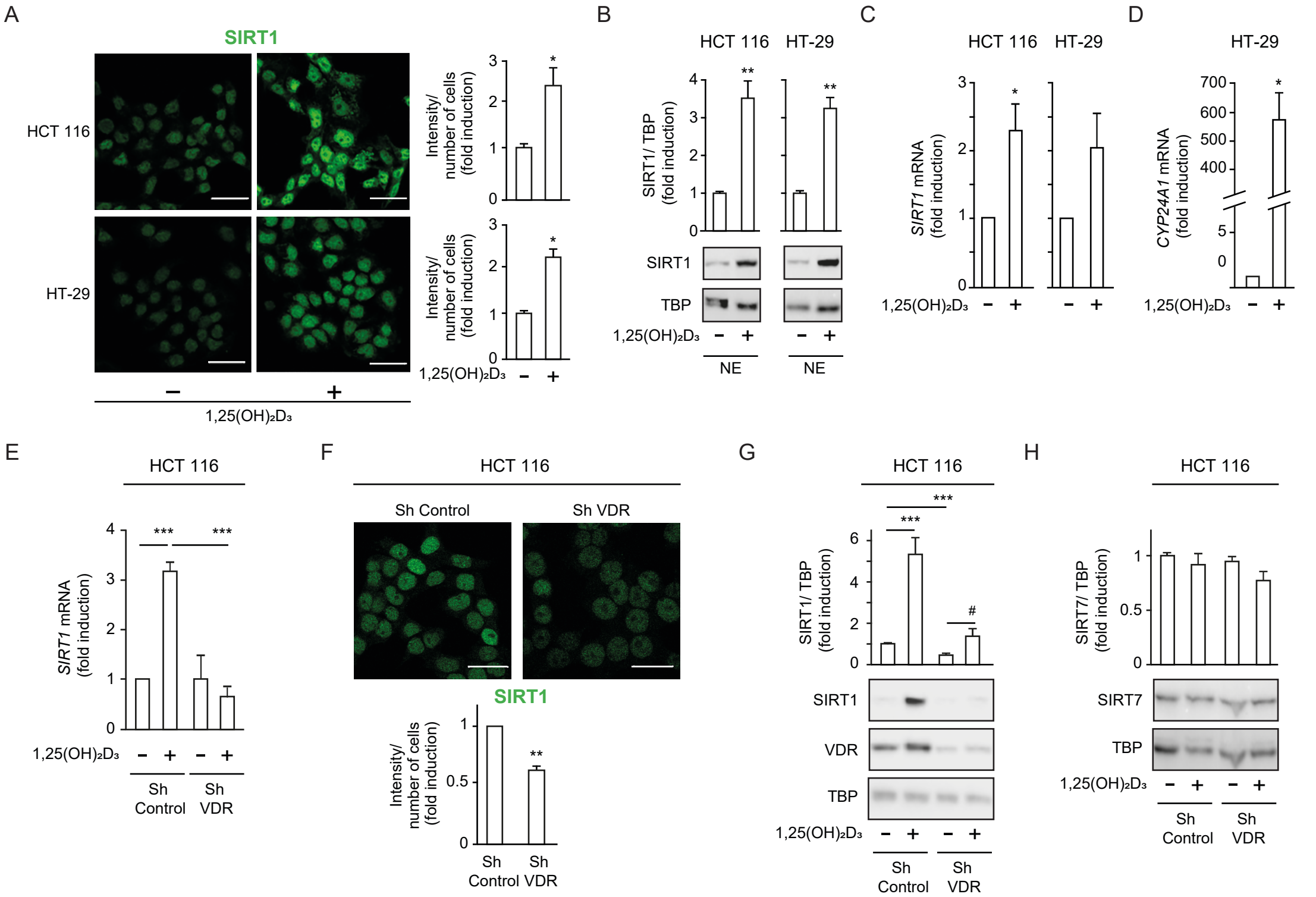
A
SIRT1
HCT 116
HT-29
Intensity/ number of cells (fold induction)
1,25(OH)₂D₃
B
HCT 116
HT-29
SIRT1/ TBP (fold induction)
SIRT1
TBP
NE
C
SIRT1 mRNA (fold induction)
D
CYP24A1 mRNA (fold induction)
E
SIRT1 mRNA (fold induction)
Sh Control
Sh VDR
F
Sh Control
Sh VDR
G
SIRT1/ TBP (fold induction)
VDR
H
SIRT7/ TBP (fold induction)
SIRT7

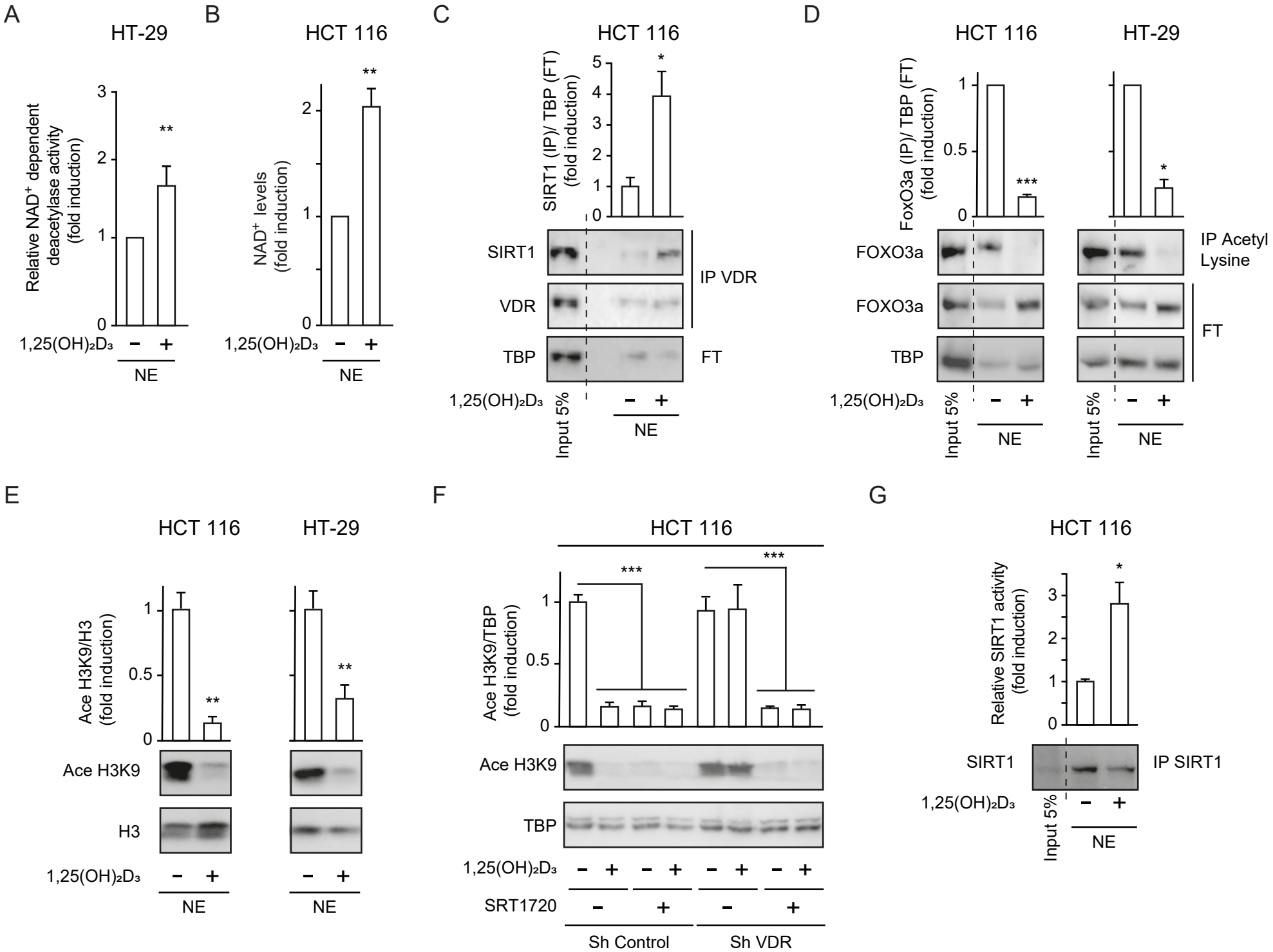
A
HT-29
Relative NAD+ dependent deacetylase activity (fold induction)
1,25(OH)2D3
NE
B
HCT 116
NAD+ levels (fold induction)
C
HCT 116
SIRT1 (IP)/ TBP (FT) (fold induction)
SIRT1
VDR
TBP
IP VDR
FT
Input 5%
D
HCT 116
HT-29
FoxO3a (IP)/ TBP (FT) (fold induction)
FOXO3a
IP Acetyl Lysine
E
Ace H3K9/H3 (fold induction)
Ace H3K9
H3
F
Ace H3K9/TBP (fold induction)
SRT1720
Sh Control
Sh VDR
G
Relative SIRT1 activity (fold induction)
IP SIRT1

A

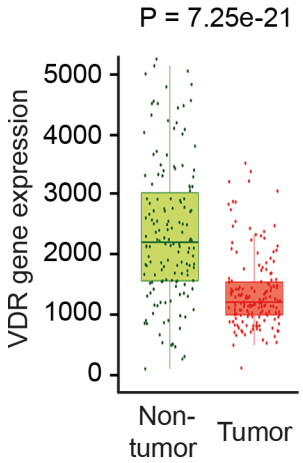

B

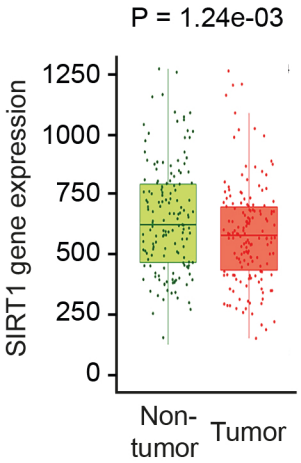

C

P = 0.017

		Tumor samples: SIRT1 protein level			
		High		Low	
		n	%	n	%
VDR protein level	High	36	56.3	32	36.8
	Low	28	43.7	55	63.2
	Total	64	100	87	100

D

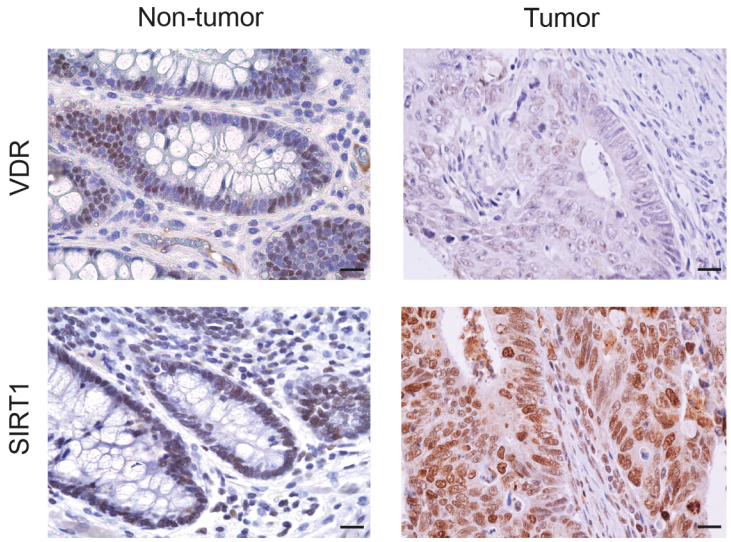

E

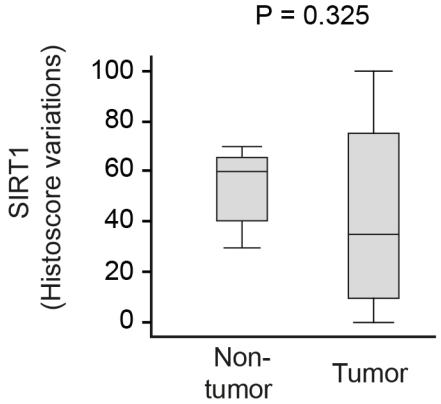

G

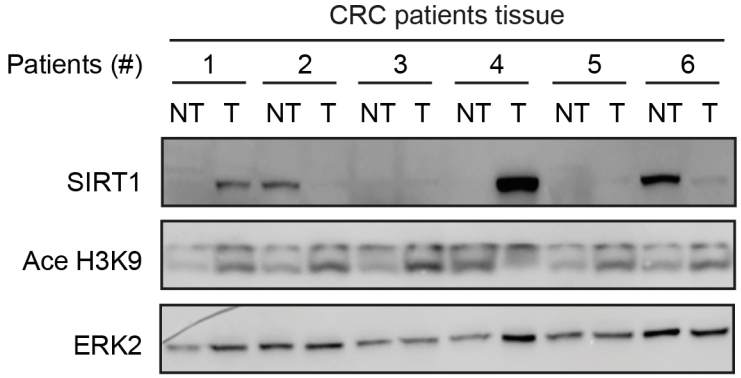

I

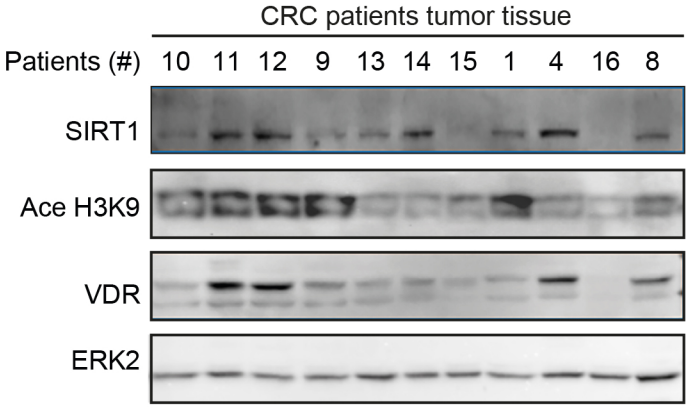

F

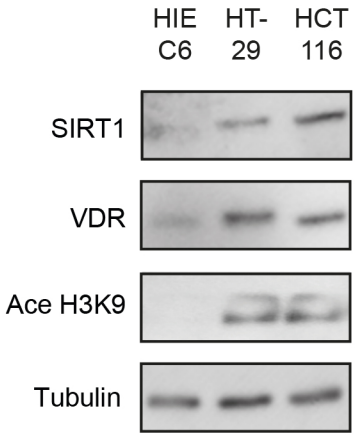

H

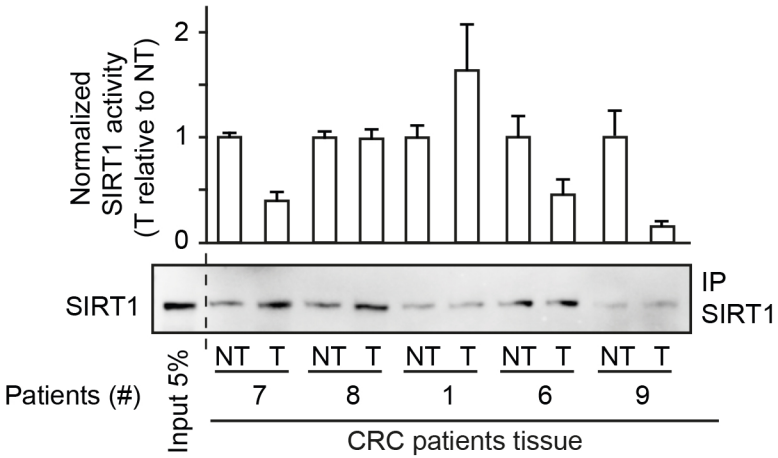

J

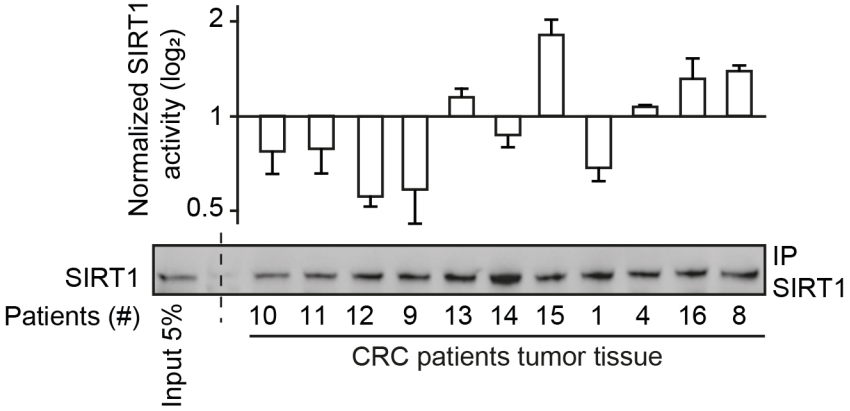

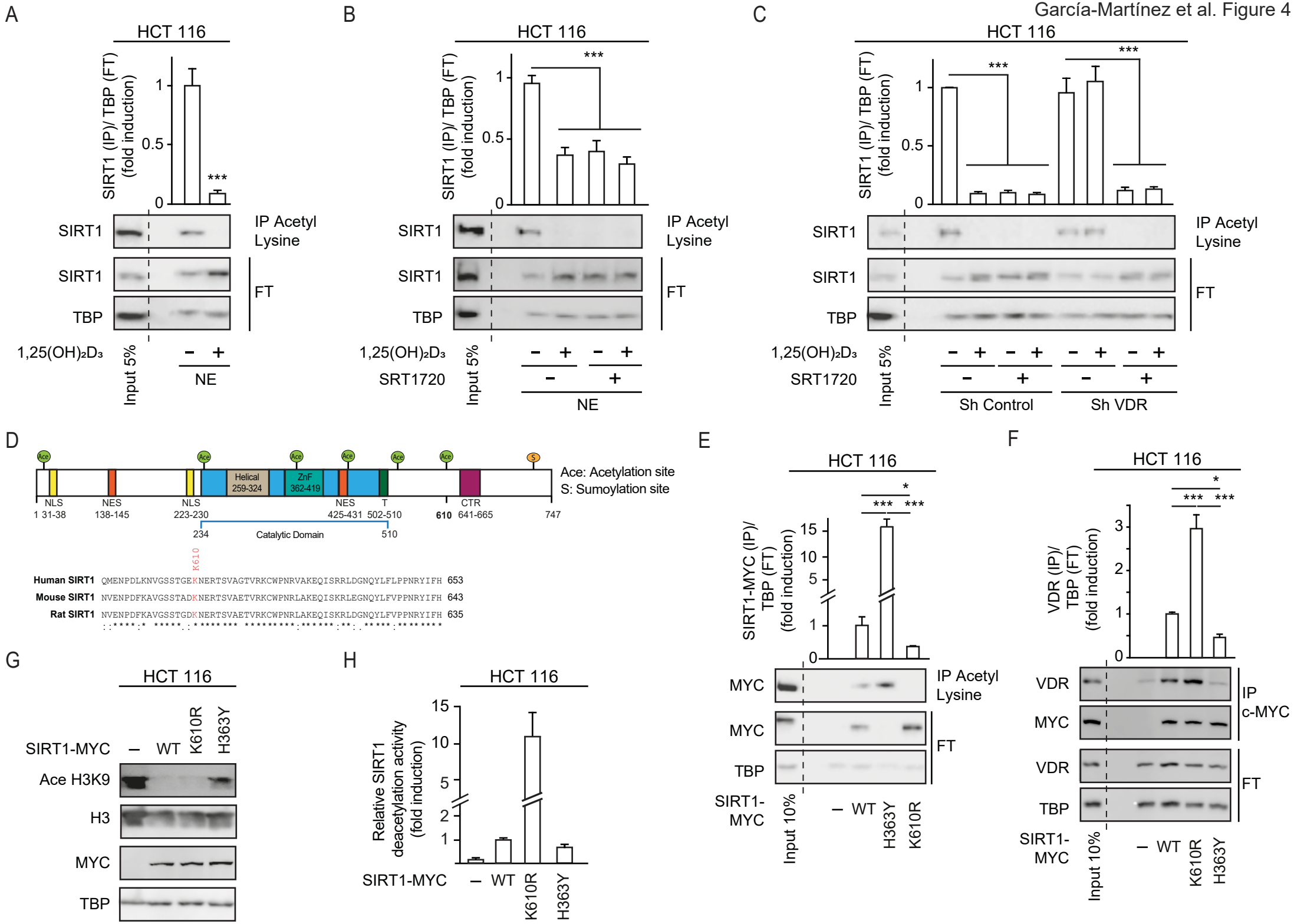
A
HCT 116
SIRT1 (IP)/ TBP (FT) (fold induction)
***
SIRT1
SIRT1
TBP
IP Acetyl Lysine
FT
1,25(OH)₂D₃
Input 5%
NE
B
HCT 116
***
SIRT1 (IP)/ TBP (FT) (fold induction)
SIRT1
SIRT1
TBP
IP Acetyl Lysine
FT
1,25(OH)₂D₃
SRT1720
Input 5%
NE
C
HCT 116
***
***
SIRT1 (IP)/ TBP (FT) (fold induction)
SIRT1
SIRT1
TBP
IP Acetyl Lysine
FT
1,25(OH)₂D₃
SRT1720
Input 5%
Sh Control
Sh VDR
D
Ace: Acetylation site
S: Sumoylation site
Helical 259-324
ZnF 362-419
NLS 1 31-38
NES 138-145
NLS 223-230
NES 425-431
T 502-510
610
CTR 641-665
747
234
Catalytic Domain
510
K610
Human SIRT1 QMENPDLKNVGSSTGEKNERTSVAGTVRKCWPNRVAKEQISRRLDGNQYLFLPPNRYIFH 653
Mouse SIRT1 NVENPDFKAVGSSTADKNERTSVAETVRKCWPNRLAKEQISKRLEGNQYLFVPPNRYIFH 643
Rat SIRT1 NVENPDFKAVGSSTGDKNERTSVAETVRKCWPNRLAKEQISKRLDGNQYLFVPPNRYIFH 635
E
HCT 116
*
***
***
SIRT1-MYC (IP)/ TBP (FT) (fold induction)
MYC
MYC
TBP
IP Acetyl Lysine
FT
SIRT1-MYC
Input 10%
WT
H363Y
K610R
F
HCT 116
*
***
***
VDR (IP)/ TBP (FT) (fold induction)
VDR
MYC
VDR
TBP
IP c-MYC
FT
SIRT1-MYC
Input 10%
WT
K610R
H363Y
G
HCT 116
SIRT1-MYC
WT
K610R
H363Y
Ace H3K9
H3
MYC
TBP
H
HCT 116
Relative SIRT1 deacetylation activity (fold induction)
SIRT1-MYC
WT
K610R
H363Y

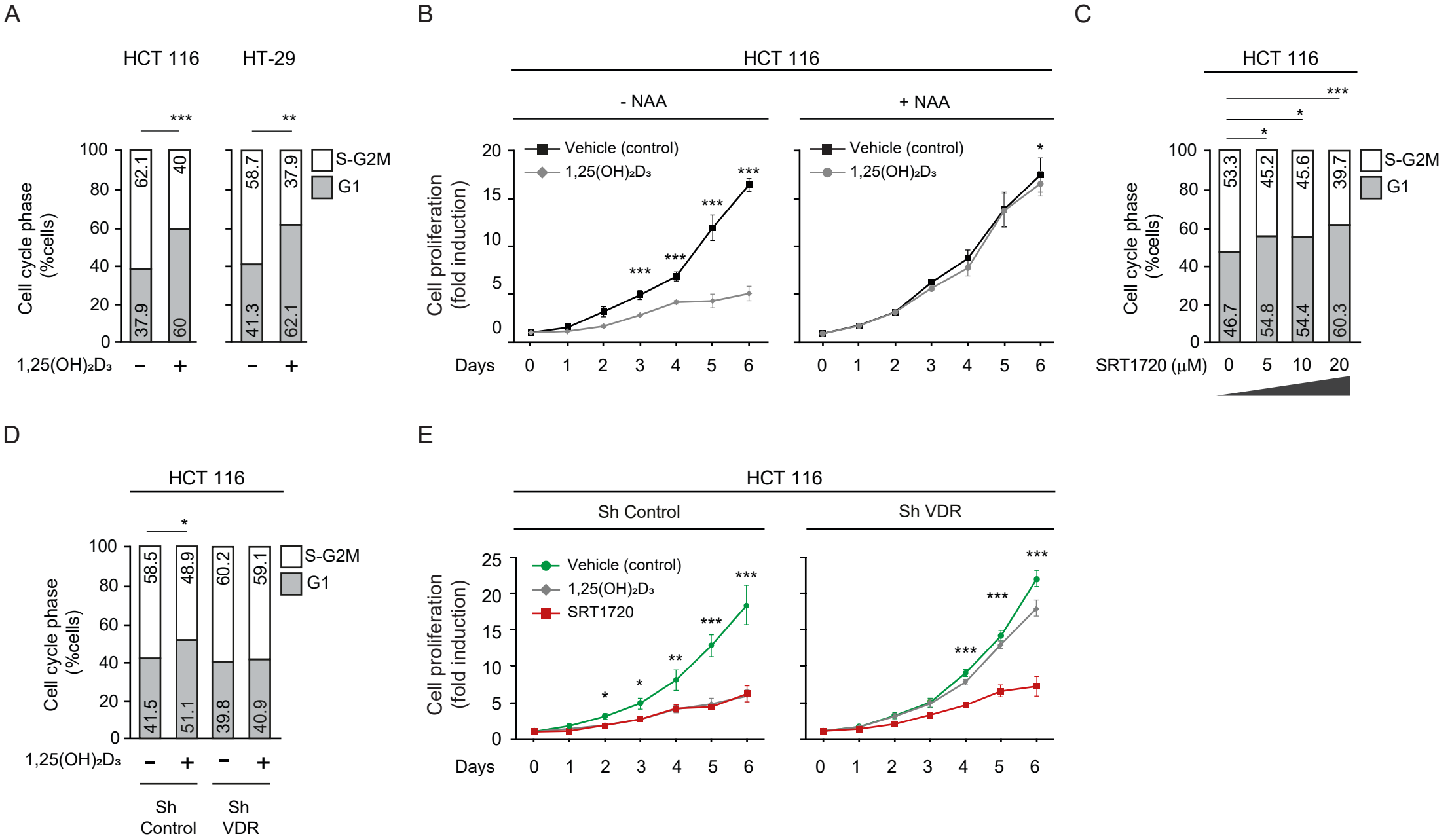
A
HCT 116
HT-29
Cell cycle phase (%cells)
S-G2M
G1
1,25(OH)₂D₃
B
HCT 116
- NAA
+ NAA
Vehicle (control)
1,25(OH)₂D₃
Cell proliferation (fold induction)
Days
C
HCT 116
SRT1720 (μM)
D
HCT 116
Sh Control
Sh VDR
E
HCT 116
Sh Control
Sh VDR
Vehicle (control)
1,25(OH)₂D₃
SRT1720